RESOURCE GEOLOGY

doi: 10.1111/rge.12009 *Resource Geology* Vol. 63, No. 3: 288–312

## Original Article

# Ages and Sources of Ore-Related Porphyries at Yongping Cu–Mo Deposit in Jiangxi Province, Southeast China

Xiaofeng Li,[1] Yasushi Watanabe[2] and Xiankui Yi[3]

[1]*Institute of Geochemistry, Chinese Academy of Sciences, Guiyang, China,* [2]*Institute for Geo-Resources and Environment, AIST, Tsukuba, Japan and* [3]*Jiangxi Institute of Geological Exploration for Mineral Resources of Nonferrous Metals, Nanchang, Jiangxi, China*

**Abstract**

Whole-rock geochemistry, zircon U–Pb and molybdenite Re–Os geochronology, and Sr–Nd–Hf isotopes analyses were performed on ore-related dacite porphyry and quartz porphyry at the Yongping Cu–Mo deposit in Southeast China. The geochemical results show that these porphyry stocks have similar REE patterns, and primitive mantle-normalized spectra show LILE-enrichment (Ba, Rb, K) and HFSE (Th, Nb, Ta, Ti) depletion. The zircon SHRIMP U–Pb geochronologic results show that the ore-related porphyries were emplaced at 162–156 Ma. Hydrothermal muscovite of the quartz porphyry yields a plateau age of 162.1 ± 1.4 Ma (2σ). Two hydrothermal biotite samples of the dacite porphyry show plateau ages of 164 ± 1.3 and 163.8 ± 1.3 Ma. Two molybdenite samples from quartz+molybdenite veins contained in the quartz porphyry yield Re–Os ages of 156.7 ± 2.8 Ma and 155.7 ± 3.6 Ma. The ages of molybdenite coeval to zircon and biotite and muscovite ages of the porphyries within the errors suggest that the Mo mineralization was genetically related to the magmatic emplacement. The whole rocks Nd–Sr isotopic data obtained from both the dacite and quartz porphyries suggest partial melting of the Meso-Proterozoic crust in contribution to the magma process. The zircon Hf isotopic data also indicate the crustal component is the dominated during the magma generation.

**Keywords:** Cu–Mo porphyry, geochronology, magma source, Southeast China, Sr–Nd–Hf isotopes, Yongping deposit.

## 1. Introduction

The Yongping Cu–Mo deposit is located 200 km east of Nanchang, the capital city of Jiangxi Province, China. The deposit occurs between the Yangtze Cu–Mo metallogenic belt and the south Jiangxi W–Sn–REE metallogenic belt (Jiangxi Geological Exploration Bureau, abbreviated as JGEB, 1996). Its location is close to a bend of the regional Jiangshan-Shaoxing fault, a Neo-Proterozoic suture zone between Yangtze and Cathaysa cratons (Fig. 1). The Cu orebodies at the Yongping deposit were discovered in the 1960s. Open-pit mining started in 1984. The Mo orebodies were discovered in 2007 with an average grade of 0.1%. As publically reported, a total of 3.4 Mt ores with a grade of 0.6% Cu and 0.1% Mo were yielded in 2007.

Studies on structural and ore geology, mineralization, geochronology, and hydrothermal alteration have been conducted at the Yongping Cu–Mo deposit (Gu & Xu, 1986; Liu & Huang, 1991; He, 1993; Ding *et al.*, 2005;

Received 12 May 2012. Accepted for publication 18 September 2012.
Corresponding author: X. Li, Institute of Geochemistry, Chinese Academy of Sciences, 46 Guanshui Road, Guiyang 550002, Guizhou, China. Email: x-f-li@hotmail.com

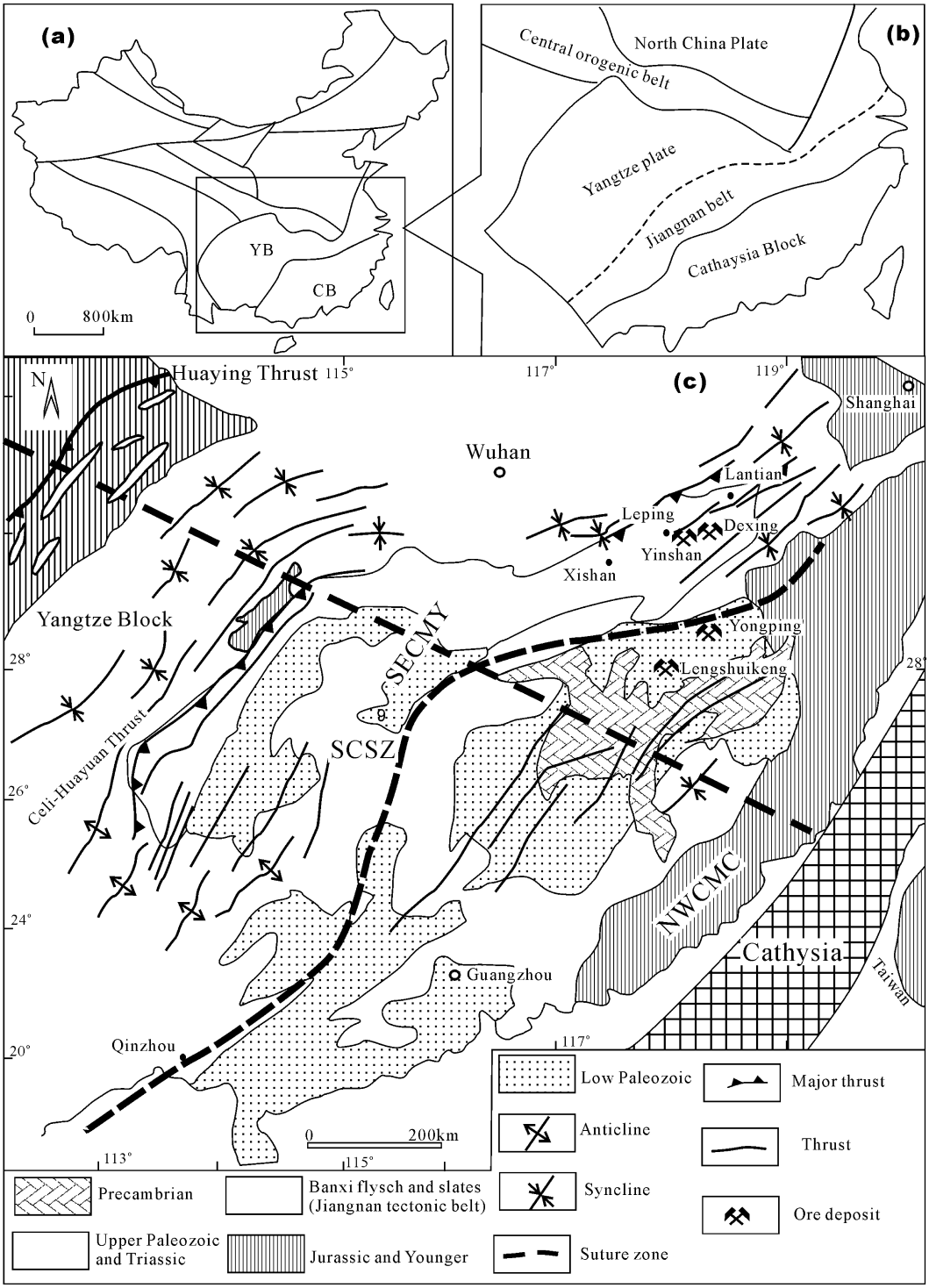


**Fig. 1** Simplified maps showing tectonic (a and b) and geologic (c) setting and the location of the Yongping Cu–Mo deposit and adjacent, major Cu-polymetallic deposits (c) in Jiangxi Province, southeast China. SECMY = the southeast continental margin of Yangtze craton (block, plate); NWCMC = the northwest continental margin of Cathaysia craton (block, plate); SCSZ = the South China Suture Zone; YB = Yangtze Block (craton, plate); CB = South China Block (plate) (modified after Chen, 1999).

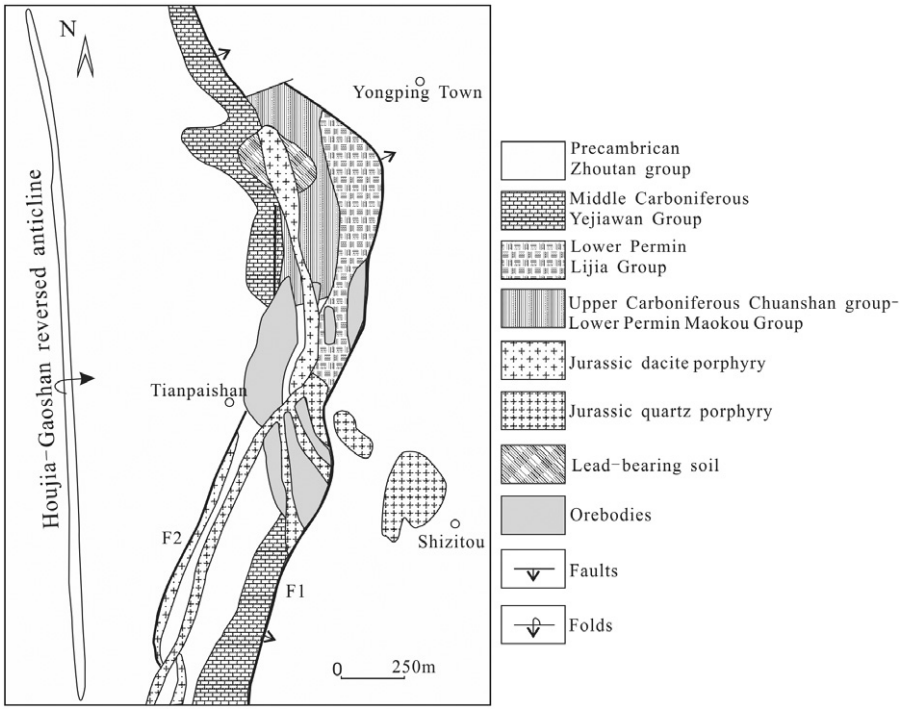


**Fig. 2** Simplified geological map of Yongping Cu–Mo deposit (modified after Huang *et al*., 2001).

Du, 2005; Li *et al*., 2007a). The arguments of the genesis of the deposit have been controversial; the deposit formed by migmatization (He, 1993), metamorphic in origin (Ren, 1994) and mixed origin of sedimentary exhalative (SEDEX) and porphyry mineralization (Gu & Xu, 1986; Liao & Liu, 2003; Du, 2005). However the published geochemical data do not support SEDEX model because the sulfur isotopes of sulfide minerals show considerable discrepancy with that in the host rocks of the Carboniferous Yejiawan Group. The source of magmas, the temporal relationship between the magmatism, hydrothermal alteration, and mineralization at the Yongping deposit remain unclear. This paper reports ion microprobe (SHRIMP) zircon U–Pb ages for the intrusive stocks in the deposit, hydrothermal muscovite and biotite $^{40}Ar$–$^{39}Ar$ ages, and molybdenite Re–Os ages. The Sr–Nd–Hf isotopes are also analyzed and presented. Their implications in the source of magmas and the origin of the deposit, as well as in regional metallogeny, are discussed.

## 2. Geology of the Yongping Cu–Mo deposit

The basement rocks in the Yongping deposit and vicinities are the Pre-Cambrian Zhoutan Group, which consists of metamorphosed shallow marine siltstone interbedded with intermediate-acidic volcanic rocks. The Middle Carboniferous Yejiawan Group is composed of littoral clastic sedimentary rocks and carbonate rocks interbedded with pyroclastic rocks; the Lower Permian Maokou Group is composed of limestone and marble, and silty shale and siltstone (Fig. 2).

The inverted Houjia-Gaoshan anticline and a number of axial faults occur at its eastern limb (such as F1 and F2) in the Yongping district (Liu & Huang, 1991). The axial faults and the anticline axis strike NNW in the north of the district and in NNE in the south of the district. In the middle of the district are several faults that strike N–S. The overall structural framework protrudes to the east (Fig. 2). The axial plane of the Houjia-Gaoshan anticline shows a dip angle of 20–30°. On the east limb of the Houjia-Gaoshan anticline is a second-order inverted syncline, named the Daziping syncline. Its exposed structural nose is 1200 m long, and it strikes N–S at a dip of 30–40°.

The location of orebodies is controlled by both F1 and F2 thrust faults. The NS-trending F1 Fault dips 15–40° east. The Zhoutang migmatite was thrusted westward over the Carboniferous-Permian stratum along the F1 Fault. The orebodies in the deposit occur

along the F1 and F2 Faults. The F2 fault is parallel to the F1 fault and exists between the Zhoutang and Yejiawan Groups. It is 5000 m long and dips 60–70° east. The Jurassic quartz porphyry was emplaced along the F2 Fault.

Igneous activities in the district include Silurian granitic porphyry and Jurassic dacite porphyry and quartz porphyry. They were emplaced into the Pre-Cambrian and Cambrian migmatite and the Middle-Carboniferous Yejiawan marine clastic rocks (Liu & Huang, 1991). The Jurassic dacite porphyry with porphyritic texture and/or quartz eye structure was related to the Cu mineralization. Phenocrysts are mainly euhedral plagioclase, platy biotite, and quartz, with minor apatite. The quartz phenocrysts are corroded to produce quartz-eye texture. The groundmass is composed of quartz, K-feldspar, plagioclase, biotite, calcite, fluorite, and magnetite. The Jurassic quartz porphyry with quartz unidirectional solidification textures (USTs) was related to Mo mineralization. Phenocrysts are mainly composed of feldspar and quartz. The groundmass is composed of quartz, feldspar, and fluorite. The volatile-rich minerals, such as fluorite, occur along the boundary between the quartz and K-feldspar (Li *et al*., 2007a).

## 3. Mineralization at the Yongping deposit

The Yongping Cu–Mo deposit is dominantly hosted by marine clastic rocks of the Carboniferous Yejiawan Group. The N–S-trending orebodies dip east at 20°–50°. They are in stratified or layered-lensoidal forms with massive and disseminated ores. Seven ore zones have been identified. Each of them is composed of multiple orebodies. The II, III, and IV zones are dominated by chalcopyrite; the V and VI zones by pyrite; and the VII zone by Cu-bearing earth and accumulates produced by secondary surface leaching. Lead- and zinc-bearing orebodies occur in the II, III, IV ore zones in the north. The thickness of the orebodies gradually changes with dip direction. The II zone is the largest in the deposit (Huang *et al*., 2001) (Fig. 2). The ore minerals are chalcopyrite, pyrite, galena, sphalerite, molybdenite, scheelite and magnetite. The gangue minerals are quartz, fluorite, calcite, garnet, anhydrite and barite.

The dacite and quartz porphyries show different ore and alteration mineral assemblages. Illitation, flurotization, biotitization, and chloritization are present in the dacite porphyry. The alteration associated with the dacite porphyry occurs along the faults. The faults contain quartz veins with pyrite. Close to the contact between the dacite porphyry and the quartz porphyry, biotitization becomes dominant in the dacite porphyry. The majority of igneous biotite are altered to chlorite and illite, and rutile seggregation along biotite cleavages is observed. The hydrothermal biotite occurs as tiny scales. Feldspar phenocrysts within the igneous rocks are altered to sericite, but their crystal shape is preserved.

The alteration of the quartz porphyry includes illitation, muscovitation, and fluorization; they occur mostly along faults and are pervasive. The feldspars are completely altered to illite and/or muscovite. Some illite recrystallized to become muscovite with diameter of 0.1–5 mm. Muscovite kinking and muscovite fish are common, indicative of a syn-tectonic alteration and mineralization. Muscovite is closely associated with molybdenite in the deposit. Molybdenite-bearing quartz veins and molybdenite veins, as well as quartz+tourmaline veins are documented in the quartz porphyry (Fig. 3). Some molybdenite-bearing quartz veins truncate the quartz porphyry and the dacite porphyry.

The porphyries are associated with skarn along their contact zones with the Yejiawan Group carbonate rocks. The skarn minerals include diopside, tremolite, actinolite, and epidote. The skarn is closely associated with the mineralization. Where garnet co-exists with diopside, tremolite, actinolite, and epidote, chalcopyrite and pyrite are present along with Pb–Zn mineralization. Where the skarn is composed of garnet only, there exist veinlets associated with chalcopyrite and pyrite. Chloritization, sericitization, and silicification overprint on the skarn, followed by carbonate, anhydrite, and fluorite precipitation. Quartz, chalcopyrite, and sphalerite veins are also observed as very late products.

Hydrothermal breccia composed of country rocks is present along the contact between the intrusive rocks and host rocks. They are cemented by fluorite, calcite, kaolinite.

## 4. Sampling and analytical procedures

Representative samples of the dacite and quartz porphyries, as well as molybdenite-bearing quartz veins were collected from the deposit. The samples were crushed and milled and heavy mineral concentrates were magnetically separated. Inclusion-free zircons,

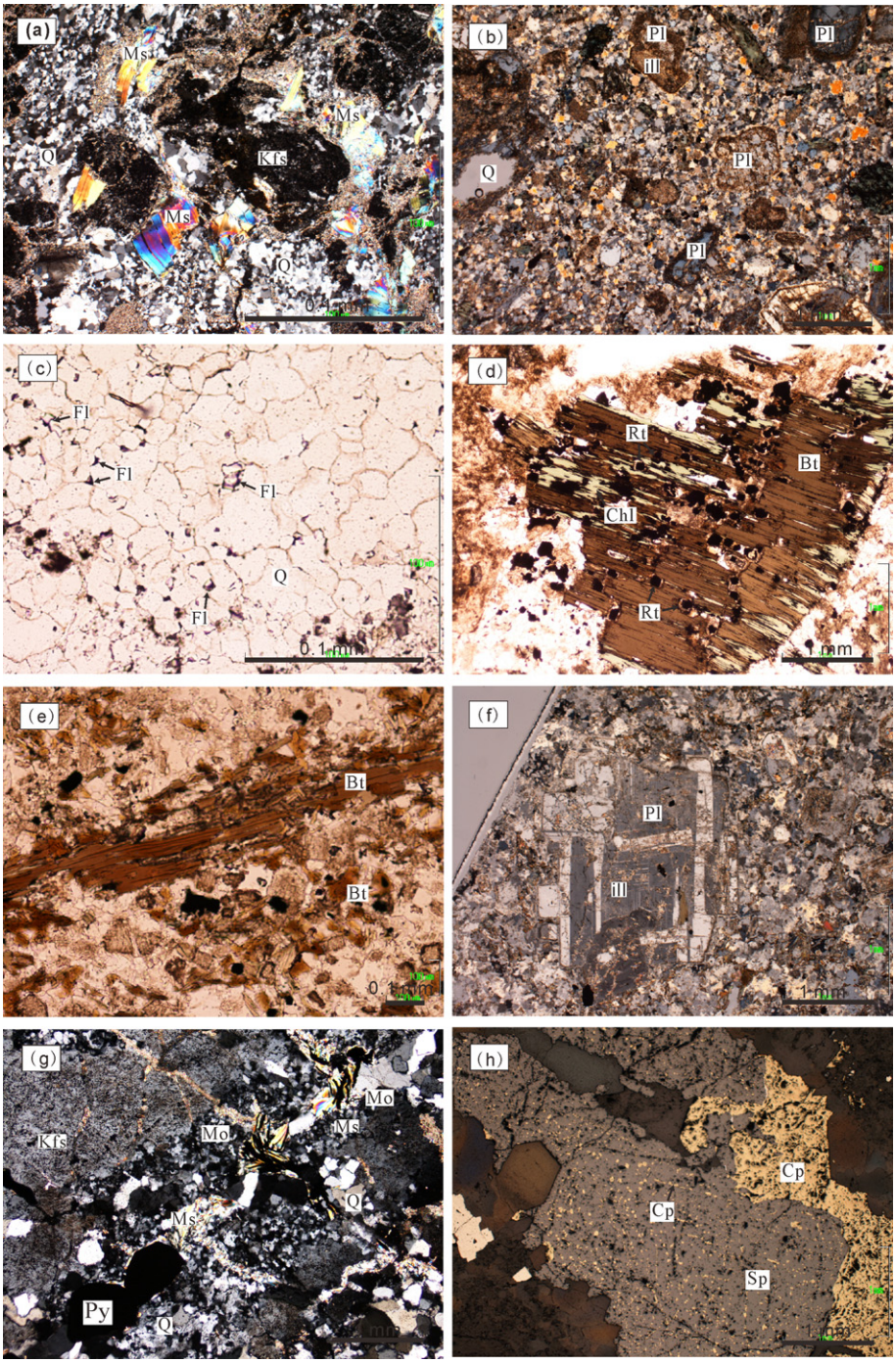


**Fig. 3** Photomicrographs of the hydrothermally altered igneous rocks of the Yongping Cu–Mo deposit. (a) Muscovite in quartz porphyry; the muscovite shows kinking. (b) Feldspar phenocryst conversion to illite within dacite porphyry. (c) Fluoritization occurs along the boundary of quartz grains and K-feldspar grains in the quartz porphyry. (d) Chloritization and exsolution of rutile from biotite phenocrysts in the dacite porphyry. (e) Biotite flakes in the dacite porphyry. (f) The least altered feldspar; sericitization occurs only along its fractures in the dacite porphyry. (g) Mo mineralization in quartz porphyry with muscovitization. (h) Chalcopyrite was replaced by sphalerite in quartz vein in dacite porphyry. Bt-biotite; Chl-chlorite; Cp-chalcopyrite; Fl-fluorite; ill-illite; Kfs-K-feldspar; Q-quartz; Pl-plagioclase; Mo-molybdenite; Ms-muscovite; Sp-sphalerite; Rt-rutile.

muscovite, biotite, and molybdenite were then hand-picked under the binocular microscope.

## 4.1 Descriptions of the samples collected for geochronologic analysis

*4.1.1 Sample YP-8*

Strongly altered quartz porphyry with unidirectional solidification texture (UST). It is composed of feldspar (40%), quartz (40%), sericite (10%), and fluorite (10%) with minor zircon, topaz and apatite. Feldspar is mostly altered to muscovite at a size of 2–5 mm. Quartz shows mosaic texture. Fine fluorite occurs along quartz grain boundaries.

*4.1.2 Sample YP-9*

Strongly altered granitic porphyry with UST, and mineralized. It is composed of K-feldspar (40%; with 2V(-) = 40), quartz (40%), calcite (10%), as well as sulfide (5%;, e.g. pyrite). Minor amount of molybdenite (1%), zircon, cassiterite and rutile (1%), and fluorite (2%) found within quartz grains.

*4.1.3 Sample YP06-16*

Weakly altered dacite porphyry with porphyritic texture. Phenocrysts (30%) are mainly euhedral plagioclase (15%), platy biotite (6%), hornblende (2%), and quartz (6%), with minor apatite (<1%). Most plagioclase phenocrysts are completely altered to sericite, and hornblende is altered to chlorite and rutile. The quartz phenocrysts are corroded to produce quartz-eye texture. The groundmass (70%) is composed of quartz, K-feldspar, plagioclase, biotite, calcite, and fluorite. K-feldspar and plagioclase are considerably altered to sericite and other clay minerals.

*4.1.4 Sample YP06-17*

Weakly altered dacite porphyry with porphyritic texture. Phenocrysts (20%) consist of euhedral plagioclase (14%), platy biotite (4%), and quartz (2%). The plagioclase phenocrysts are partially altered to sericite, and the quartz is rounded with corroded structure. The groundmass consists of anhedral quartz (40%), euhedral-subhedral plagioclase (24%), anhedral K-feldspar (8%), and biotite (8%), with trace apatite (<1%).

*4.1.5 Sample YP06-18*

Least altered quartz porphyry with quartz UST structure (Kirwin, 2005, 2006). It is mainly composed of feldspar including large phenocrysts of K-feldspar (with 2V(-) = 30–60°, 4–5 mm in diameter), quartz, calcite, and fluorite with trace pyrite and chalcopyrite. Quartz shows mosaic texture. Feldspar crystals are partially altered to clay minerals such as sericite. Fluorite occurs along the boundaries of quartz.

*4.1.6 Sample YP06-4*

Weakly altered quartz porphyry with quartz UST structure. It is mainly composed of K-feldspar, plagioclase, and quartz. Plagioclase phenocrysts are altered to sericite clay minerals. Opaque minerals include pyrite, radial rutile, molybdenite, as well as fluorite.

*4.1.7 Samples YP-10 and YP-2*

Collected from two quartz+molybdenite veins within the quartz porphyry.

## 4.2 Whole-rock geochemical analysis

Two criteria were used for the sample selection from outcrops within the ore-hosting porphyries: (i) homogeneous samples and (ii) samples with the least effects of hydrothermal alteration based on petrographic observations. There were 9 samples collected for whole-rock geochemical analysis. Sample preparation was carried out by jaw-crushing and grinding in a ring mill. Major elements were analyzed by X-ray fluorescence spectroscopy (XRF). Trace elements were analyzed by inductively coupled plasma-mass spectrometry (ICP-MS) and the FeO was analyzed with titration methods, F with ionselective electrode (ISE) method, and S with infrared method. All the whole-rock analyses were performed at the Activation Laboratories Ltd. in Canada. Details of the chemical procedures are accessible at http://www.actlabs.com.

## 4.3 Whole-rock Rb-Sr and Sm-Nd isotopes

Rb–Sr and Sm–Nd isotope compositions of the whole-rock samples selected from the ore-hosting porphyries were determined by using a GV IsoProble-T multi-collector thermal ionization mass spectrometer at the Geological Institute of Nuclear Industry in Beijing, China, following the method of Zhang *et al*. (1994). $^{87}Sr/^{86}Sr$ and $^{143}Nd/^{144}Nd$ ratios are reported as normalized to $^{86}Sr/^{88}Sr$ of 0.1194 for Sr and to $^{146}Nd/^{144}Nd$ of 0.7219 for Nd. Measurements for the Johnson Mattey $Nd_2O_3$ standard and for NBS-987 Sr standard yielded results of $^{143}Nd/^{144}Nd$ ratios of $0.511126 \pm 9$ ($2\sigma$, $n = 27$),

and $^{87}Sr/^{86}Sr$ ratios of 0.710228 ± 14 (2σ, $n = 30$), respectively. Total analytical blanks were $5 \times 10^{-11}$g for Sm and Nd, and (2–5) $\times 10^{-10}$g for Rb and Sr.

Initial $^{86}Sr/^{87}Sr$ ratios ($I_{Sr}$ or $(^{86}Sr/^{87}Sr)_o$) were calculated at time t with $^{87}Rb$ decay constant of $1.42 \times 10^{-11}$ (Steiger & Jäger, 1977). Initial $^{143}Nd/^{144}Nd$ ratios with reference to chondritic reservoir (CHUR) at the time t of rock-formation. The $^{147}Sm$ decay constant of $6.54 \times 10^{-12}$ (Lugmair & Marti, 1978) and the present-day chondritic ratios of $^{143}Nd/^{144}Nd = 0.512638$ (Goldstein *et al*., 1984) and $^{147}Sm/^{144}Nd = 0.1967$ (Peucat *et al*., 1989) were adopted in this analysis. $\varepsilon_{Nd}(t)$ is the measure parameter of the difference between the $^{143}Nd/^{144}Nd$ ratios of a sample at time of its formation and a reference chondritic reservoir. Single-stage model ages ($T_{DM1}$) were calculated relative to the depleted mantle ($^{147}Sm/^{144}Nd = 0.2137$, $^{143}Nd/^{144}Nd = 0.51315$, Peucat *et al*., 1989). Two-stage model ages ($T_{DM2}$) were also calculated assuming a $^{147}Sm/^{144}Nd$ ratio of 0.118 for the continental crust (Jahn & Condie, 1995).

### 4.4 SHRIMP U-Pb dating

Zircon grains were selected from four samples (YP-9, YP06-16, YP06-17, and YP06-18) of the granite porphyry, dacite porphyry and quartz porphyry in the Yongping deposit. The selected zircons and the G1939 reference zircons were mounted in epoxy before sectioned approximately in half and polished. Reflected, transmitted optic photomicrographs, BSE images, and cathodoluminescence (CL) images were obtained for all zircon samples. The CL images were used to examine internal structure of zircons and to ensure that the 20 μm SHRIMP spot was within a single component of a zircon.

The U-Pb isotopic analysis was performed using SHRIMP-II at the SHRIMP Center at the Institute of Geology of the Chinese Academy of Geological Sciences in Beijing, following the procedure described by Jian *et al*. (2003). For each zircon, its $Zr_2O^+$, $^{204}Pb^+$ background, $^{206}Pb^+$, $^{207}Pb^+$, $^{208}Pb^+$, $U^+$, $Th^+$, $ThO^+$, and $UO^+$ were measured on a single electron multiplier by cyclic magnetic field stepping. The mean ion counts were measured and recorded every five scans. A primary ion beam of ~4.5 nA, 10 kV $O^{2-}$, and ~25–30 μm spot diameter was used. Inter-element fraction in the ion emission of zircon was corrected using the RSES reference standard TEM. The software of Ludwig (SQUID 1.0) and accompanying ISOPLOT were used for data processing and plotting (Ludwig, 2001). Ages were calculated by using the constants recommended by IUGS (Steiger & Jäger, 1977). Unless otherwise stated, analytical uncertainties given in the table and shown in the plots have one standard deviation (1σ). The ages from polled data are weighted means, with uncertainties given at two standard deviations.

All the analyses were conducted in static mode. Inter-element fractionation was monitored analyzing fragments of 91500, a large concordant zircon crystal with a known age (SHRIMP U–Pb) of 1061 Ma. This reference zircon was analyzed once for every three unknown samples. The reported ages for zircon grains are based on $^{206}Pb/^{238}U$ ratios due to high errors of the $^{207}Pb/^{235}U$ and $^{207}Pb/^{206}Pb$ ratios. This is due primarily to the low intensity of $^{207}Pb$ signal from these young, low-U grains. The $^{206}Pb/^{238}U$ ratios are corrected for common Pb by the measured $^{206}Pb/^{204}Pb$.

For each sample, the $^{206}Pb/^{238}U$ ages are plotted with 2σ error bars that reflect only the error from determined $^{206}Pb/^{238}U$ and $^{206}Pb/^{204}Pb$. For the age of each sample, additional uncertainty from the calibration, decay constant, common lead composition, and variations in the measured $^{206}Pb/^{238}U$ and $^{206}Pb/^{207}Pb$ from 91500 standard is considered. These systematic errors were added quadratically to the measurement error. All the reported ages and weighted mean ages have uncertainties at the 2σ level. Weighted mean $^{206}Pb/^{238}U$ ages were calculated, and the uncertainties are reported as 95% confidence limit.

### 4.5 Zircon Hf isotopes

Zircon Hf isotope analysis was carried out in-situ using a Geolas-193 laser-ablation microprobe attached to a Neptune multi-collector ICFMS, at the Institute of Mineral Resources, Chinese Academy of Geological Sciences, Beijing. Instrumental conditions and data acquisition were described by Xu *et al*. (2004). The laser system is equipped with a 193n UV ArF excimer laser. Typical ablation time for each analysis is about 30 s for 200 cycles of each measurement, with a 10 Hz repetition rate, and a laser power of 100 mJ/pulse. A stationary spot was used for the analysis, with a beam diameter of about 63 μm. Both He and Ar carrier gases were used to transport the ablated materials from the laser-ablation cell via a mixing chamber to the ICP torch. Isobaric interference of $^{176}Lu$ on $^{176}Hf$ was corrected measuring the intensity of the interference-free $^{175}Lu$ isotope and using the recommended $^{176}Lu/^{175}Lu$ ratios of 0.02655 to calculate $^{176}Lu/^{177}Hf$ ratios. Correction for isobaric interference of $^{176}Yb$ on $^{176}Hf$ was

performed in real time (Wu *et al*., 2006) as developed by Iizuka and Hirata (2005). Standard zircon 91500 showed similar average $^{176}Hf/^{177}Hf$ ratios of 0.282307 ± 58, but a bimodal distribution with two peaks at 0.282284 ± 22 and 0.282330 ± 29. The Hf isotope heterogeneity in 91500 brings extra uncertainties to the data, however, our analyses on 91500 in two sessions yielded only one peak at 0.282307 ± 31 (Wu *et al*., 2006). This means that at least this chip of 91500 analyzed is homogeneous in Hf isotopes. All the Lu–Hf isotope results are reported with a 2σ error (Table 4).

Initial $^{176}Hf/^{177}Hf$ ratios ($\varepsilon_{Hf}(t)$) were calculated with reference to chondritic reservoir (CHUR) at the time t of zircon growth from magmas, the single grain zircon SHRIMP U–Pb age were used to represent the zircon growth time t from magmas for each point. The $^{176}Lu$ decay constant of $1.865 \times 10^{-11}$ $yr^{-1}$ (Nowell *et al*., 1998) and the present-day chondritic ratios of $^{176}Hf/^{177}Hf$ = 0.282772 and $^{176}Lu/^{177}Hf$ = 0.0332 (Blichert-Toft & Albarede, 1997) were adopted in this analysis. Single-stage model ages ($T_{DM1}$) were calculated relative to the depleted mantle with a present-day $^{176}Hf/^{177}Hf$ ratio of 0.28325, similar to that of the average MORB (Nowell *et al*., 1998) and a present-day $^{176}Lu/^{177}Hf$ ratio of 0.0384 (Griffin *et al*., 2000). Errors in both $\varepsilon_{Hf}(t)$ and $T_{DM1}$ values were calculated on the basis of analytical errors, but much bigger and poorly constrained errors could be associated with the Hf model ages due to uncertainties in the reference model (Nowell *et al*., 1998).

Two-stage model ages ($T_{DM2}$) were also calculated by projecting the initial $^{176}Hf/^{177}Hf$ of the zircon back to the depleted mantle model growth curve, assuming a $^{176}Lu/^{177}Hf$ ratio of 0.009 for the upper continental crust of Archean age. A $^{176}Lu/^{177}Hf$ ratio of 0.015 was assumed for the average continental crust (Griffin *et al*., 2000), which is consistent with the average $^{176}Lu/^{177}Hf$ values of Archean sedimentary rocks in Superior Province of North America (Stevenson & Patchett, 1990; Corfu & Noble, 1992).

### 4.6 Muscovite and biotite Ar-Ar dating

Muscovite samples selected from specimens YP06-4, and the hydrothermal biotite samples selected from specimens YP06-16, and YP06-17 were purified by magnetic separator and then cleaned by ultrasonic treatment with ethanol. The purity of the muscovite grains (at a size of 0.08–0.15 mm) is greater than 99%. The biotite and muscovite samples were irradiated for 51 hours in a nuclear reactor at the Chinese Institute of Atomic Energy in Beijing, and subsequently cooled for approximately 100 days. $^{40}Ar/^{36}Ar$ stepwise heating analysis was performed at the Institute of Geology, Chinese Academy of Geological Sciences using a MM-1200B Mass Spectrometer. Measured isotopic ratios were corrected for the mass discrimination, atmospheric Ar component, blanks and irradiation-induced mass interference. The decay constant used is $\delta = 5.543 \times 10^{-10}$ $year^{-1}$ (Steiger & Jäger, 1977). All $^{37}Ar$ were corrected for radiogenic decay (half-life 35.1 days). Uncertainty in each apparent age is given at 2σ. The monitor used in this analysis was an internal standard: Fangshan biotite (ZBH-25) of 132.7 Ma and its potassium content is 7.6%. The *J*-values of the monitors are given in Tables 5–7. Detailed analytical techniques are described by Chen *et al*. (2002).

### 4.7 Molybdenite Re-Os dating

Molybdenite samples were separated from molybdenite-bearing quartz veins for the Re-Os analyses following the method described by Mathur *et al*. (2002) and Barra *et al*. (2003). Approximately 0.05–0.10 g of handpicked molybdenite was loaded in a carius tube with 8 mL of reverse aqua regia (1HCl:3$HNO_3$). While the reagents, samples, and spikes were frozen, the Carius tube was sealed and left to thaw at room temperature. The tube was placed in an oven and heated to 240°C overnight. The solution was treated in a two-stage distillation process for osmium separation (Nagler & Frei, 1997). Osmium was further purified using a micro-distillation technique (Birck *et al*., 1997) and loaded on platinum filaments with $Ba(OH)_2$ to enhance ionization. After osmium separation, the remaining acid solution was dried and later dissolved in 0.1 $HNO_3$. Rhenium was extracted and purified through a two-stage column using resin and loaded on platinum filaments with $BaSO_4$.

Samples were analyzed with ICP-MS at Chinese Academy of Geological Sciences, Beijing. Molybdenite ages were calculated using a $^{187}Re$ decay constant of $1.666 \times 10^{-11}$ per year (Smoliar *et al*., 1996). Ages were reported with 0.5% error, which is considered a conservative estimate and reflects all sources of errors.

## 5 Results

### 5.1 Major and trace elements

Results of major and trace element contents of the ore-hosting quartz and dacite porphyries are listed in Table 1. Some of the analyzed samples contain variable loss on ignition (LOI) values reflecting variable

**Table 1** Geochemical data of the igneous rocks in the Yongping Cu–Mo deposit

| Samples | Quartz porphyry | | | | | Dacite porphyry | | | |
|---|---|---|---|---|---|---|---|---|---|
| | YP-4 | YP-7 | YP-8 | YP06-18 | YP06-26 | YP06-16 | YP06-17 | YP06-20 | YP06-21 |
| Wt% | | | | | | | | | |
| $SiO_2$ | 74.76 | 71.17 | 74.45 | 76.21 | 73.32 | 63.15 | 64.53 | 66.15 | 63.76 |
| $TiO_2$ | 0.19 | 0.38 | 0.06 | 0.34 | 0.41 | 0.57 | 0.66 | 0.52 | 0.55 |
| $Al_2O_3$ | 13.23 | 13.57 | 14.91 | 10.79 | 13.15 | 14.03 | 15.81 | 15.53 | 15.21 |
| $Fe_2O_3$ | 1.38 | 1.08 | 0.28 | 0.01 | 0.37 | 0.81 | 2.25 | 0.77 | 1.58 |
| FeO | 1.76 | 1.84 | 0.71 | 0.86 | 1.13 | 2.56 | 1.57 | 2.38 | 1.75 |
| MnO | 0.003 | 0.008 | 0.004 | 0.015 | 0.016 | 0.03 | 0.02 | 0.02 | 0.05 |
| MgO | 0.72 | 1.31 | 0.95 | 0.61 | 1.41 | 2.35 | 2.03 | 1.45 | 1.75 |
| CaO | 0.02 | 0.98 | 0.22 | 1.76 | 1.07 | 2.90 | 3.02 | 2.21 | 2.63 |
| $Na_2O$ | 0.09 | 0.10 | 0.10 | 0.13 | 0.11 | 0.50 | 2.74 | 0.93 | 1.86 |
| $K_2O$ | 4.51 | 5.08 | 5.34 | 5.74 | 5.64 | 6.75 | 4.29 | 5.57 | 5.33 |
| $P_2O_5$ | 0.02 | 0.08 | 0.13 | 0.10 | 0.11 | 0.16 | 0.20 | 0.20 | 0.19 |
| F | 0.19 | 1.84 | 0.20 | 0.15 | 0.17 | 0.13 | 0.12 | 0.13 | 0.10 |
| LOI | 3.43 | 4.53 | 3.41 | 2.71 | 3.25 | 5.91 | 2.71 | 4.47 | 4.26 |
| S | 2.55 | 2.19 | 0.61 | — | — | — | — | — | — |
| Total (%) | 100.2 | 100.3 | 100.3 | 99.4 | 100.1 | 100 | 100 | 100.1 | 99.1 |
| ppm | | | | | | | | | |
| Ba | 1676 | 890 | 865 | 579 | 488 | 2130 | 912 | 777 | 1490 |
| Rb | 130 | 180 | 170 | 200 | 190 | 207 | 207 | 212 | 187 |
| Sr | 14 | 61 | 38 | 90 | 63 | 251 | 251 | 190 | 299 |
| Y | 6 | 19 | 34 | 9.1 | 12.5 | 14.2 | 14.2 | 10.1 | 13.3 |
| Zr | 105 | 168 | 59 | 87 | 114 | 142 | 142 | 149 | 164 |
| Nb | — | — | — | 9.7 | 11.9 | 11.2 | 11.8 | 12.2 | 12.5 |
| Th | 6.8 | — | 7.4 | 5.45 | 7.85 | 7.02 | 7.54 | 7.96 | 8.82 |
| Pb | 26 | 5 | 16 | 5 | 7 | 5 | 5 | 7 | 9 |
| Ga | — | — | — | 14 | 16 | 19 | 21 | 21 | 20 |
| Zn | 8 | 12 | 34 | 30 | 30 | 30 | 30 | 30 | 30 |
| Cu | 637 | 85 | 27 | 40 | 20 | 220 | 110 | 240 | 50 |
| V | 31 | 67 | 13 | 53 | 69 | 83 | 83 | 67 | 70 |
| Cr | 2.1 | 23.2 | 0.5 | 20 | 20 | 30 | 20 | 20 | 20 |
| Hf | 2.3 | 3.8 | 1.2 | 2.6 | 3.2 | 3.8 | 4.3 | 3.9 | 4.4 |
| Cs | 1.1 | 3.1 | 3.9 | 5.2 | 7.1 | 7.5 | 7.7 | 12.3 | 9.8 |
| Ta | 0.5 | 0.3 | 1.1 | 0.82 | 1.07 | 0.84 | 0.87 | 0.95 | 0.99 |
| Co | 11.9 | 10.3 | 2.8 | 2 | 4 | 8 | 7 | 4 | 5 |
| U | 1.2 | 2 | 4.8 | 4.27 | 3.7 | 2.38 | 2.78 | 2.22 | 3.16 |
| W | 39 | 50 | 13 | 27.4 | 57.4 | 30 | 10.8 | 27.3 | 12.3 |
| Mo | 3 | 4 | 2 | 19 | 75 | 27 | 46 | 4 | 2 |
| La | 26.2 | 31.1 | 12.5 | 18.6 | 24.6 | 32.6 | 33.4 | 38 | 36.7 |
| Ce | 46 | 61 | 27 | 34.9 | 46.1 | 62 | 63.5 | 68.3 | 68.4 |
| Pr | — | — | — | 3.8 | 5.06 | 6.9 | 6.96 | 7.35 | 7.44 |
| Nd | 16 | 28 | 13 | 13.8 | 18.1 | 26 | 25.8 | 26.5 | 26.7 |
| Sm | 2.58 | 4.6 | 3 | 2.48 | 3.24 | 4.72 | 4.4 | 4.53 | 4.63 |
| Eu | 0.64 | 1.08 | 0.66 | 0.67 | 0.90 | 1.28 | 1.31 | 1.27 | 1.22 |
| Gd | — | — | — | 2.02 | 2.59 | 3.7 | 3.45 | 3.28 | 3.51 |
| Tb | 0.3 | 0.6 | 0.7 | 0.31 | 0.43 | 0.5 | 0.49 | 0.43 | 0.54 |
| Dy | — | — | — | 1.66 | 2.36 | 2.76 | 2.44 | 1.94 | 2.75 |
| Ho | — | — | — | 0.3 | 0.41 | 0.49 | 0.42 | 0.32 | 0.45 |
| Er | — | — | — | 0.81 | 1.08 | 1.32 | 1.08 | 0.81 | 1.2 |
| Tm | — | — | — | 0.11 | 0.15 | 0.18 | 0.14 | 0.11 | 0.16 |
| Yb | 0.53 | 1.84 | 2.69 | 0.67 | 0.97 | 1.13 | 0.82 | 0.7 | 1.01 |
| Lu | 0.08 | 0.27 | 0.40 | 0.096 | 0.15 | 0.16 | 0.12 | 0.11 | 0.14 |

Note: "—" not analyzed.

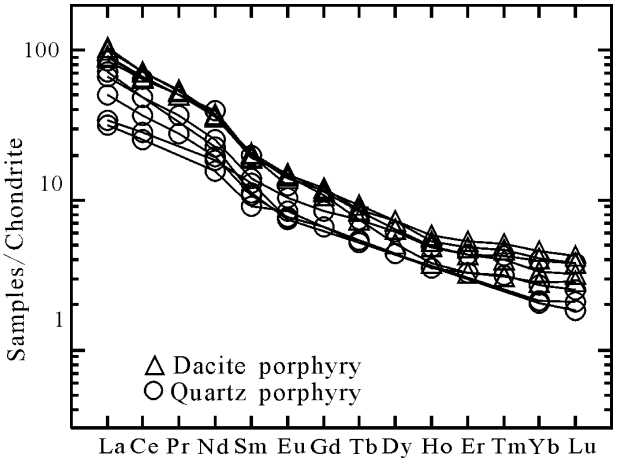


**Fig. 4** Chondrite-normalized REE diagram for both dacite and quartz porphyries, Chondritic normalization is according to Sun and McDonough (1989).

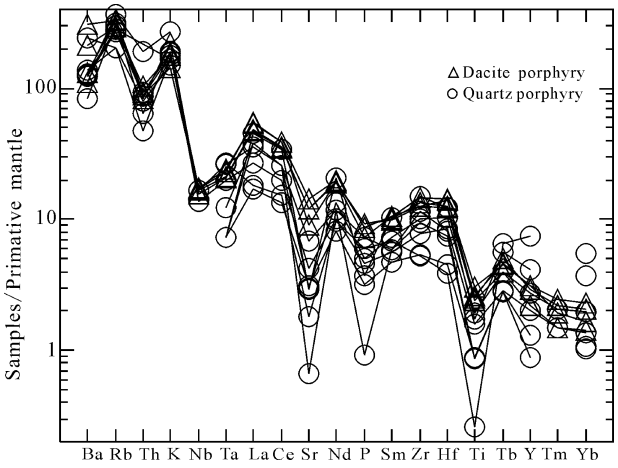


**Fig. 5** Primitive mantle-normalized trace element spider diagram for both dacite and quartz porphyries, Normalizing values are according to Sun and McDonough (1989).

$H_2O+CO_2$ contents, possibly due to different degree of alteration. In general, the high-field-strength elements (HFSE), rare earth elements (REE), and transition elements are immobile during the hydrothermal alteration (Hawkesworth *et al.*, 1997). However, the $Na_2O$ and $K_2O$ contents show a decrease and increase with increasing LOI, respectively, implying their original contents were modified by alteration. Thus, only immobile elements are used in the following discussion.

The total REE concentrations range from 118.64 ppm to 168.16 ppm in the dacite porphyries and from 56.41 ppm to 147.49 ppm in the quartz porphyries. Both porphyries are rich in light REE and poor in heavy REE. The chondrite-normalized REE diagram (Fig. 4) shows a steep curve pattern without Eu depletion. As shown in the primitive mantle-normalized trace element spider diagram (Fig. 5), both types of the porphyries are rich in large ion lithophile elements (Ba, Rb, and K), and depleted in high field strength elements (Th, Nd, Ta, and Ti) and Sr and P. This may suggests subduction-related arc magmatism. The depleted Sr and P may suggest a magma fractional crystallization process.

## 5.2 Rb–Sr and Sm–Nd isotopes

The Rb–Sr and Sm–Nd isotopic compositions of the dacite and quartz porphyries are listed in Table 2. Table 2 shows the initial Sr isotopic composition for dacite porphyry and quartz porphyry ranging from 0.707 to 0.710, and from 0.704 to 0.712, respectively. The $\varepsilon_{Nd}(t)$ values range from –9.18 to –7.64 and from –10.95 to –6.94, respectively. The Nd model ages of the dacite and quartz porphyries relative to a depleted mantle ($T_{DM1}$) range from 1.26 to 1.38 Ga (with a mean of 1.32 Ga), and from 1.24 to 1.44 Ga (with a mean of 1.30 Ga), respectively. Two-stage Nd model ages of the dacite and quartz porphyries relative to a depleted mantle ($T_{DM2}$) range from 1.57 to 1.69 Ga (with a mean of 1.63 Ga) and from 1.51 to 1.84 Ga (with a mean of 1.62 Ga), respectively.

## 5.3 Zircon SHRIMP U-Pb ages

Zircons used for SHRIMP U-Pb analysis were examined on the basis of petrographic microscopy and cathodoluminescence (CL) microscopy with a backscattered electron imaging system. Target spots were selected based on CL images (Fig. 6). Zircons are colorless and range from oval, elongate, to long elongate in shape, generally showing 101 type. Most of the zircons were devoid of inclusions, although a few contain minute inclusions.

### *5.3.1 Sample YP-9*

A total of 14 spots were analyzed on 13 zircon grains selected from sample YP-9 which was collected from strongly altered quartz porphyry. All the analyzed zircon grains have relatively uniform texture typical of metamorphic origin. Sample YP-9 yields a $^{206}Pb/^{238}U$ weighted average age of 435.2 ± 7.3 Ma ($n$ = 14 zircons, mean square of weighted deviation (MSWD) = 0.45) (Fig. 7a, Table 3).

**Table 2** Rb-Sr and Sm-Nd isotope compositions of porphyries in the Yongping Cu–Mo deposit

| Samples | Rock Types | $^{87}Rb/^{86}Sr$ | $^{87}Sr/^{86}Sr$ | $(^{87}Sr/^{86}Sr)_i$ | $^{147}Sm/^{144}Nd$ | $^{143}Nd/^{144}Nd$ | $^{143}Nd/^{144}Nd_{(t)}$ | $Nd_{CHUR(t)}$ | $\varepsilon_{Nd(t)}$ | $T_{DM1}$ (Ma) | $T_{DM2}$ (Ma) |
|---|---|---|---|---|---|---|---|---|---|---|---|
| YP06-16 | Dacite porphyry | 2.5932 | 0.71608 | 0.71029 | 0.0893 | 0.51206 | 0.51197 | 0.51244 | –9.18 | 1340 | 1693 |
| YP06-17 | Dacite porphyry | 1.1196 | 0.71093 | 0.70844 | 0.0883 | 0.51211 | 0.51202 | 0.51244 | –8.05 | 1260 | 1601 |
| YP06-20 | Dacite porphyry | 3.5494 | 0.71578 | 0.70786 | 0.0973 | 0.51210 | 0.51200 | 0.51244 | –8.60 | 1382 | 1646 |
| YP06-21 | Dacite porphyry | 2.0237 | 0.71363 | 0.70911 | 0.093 | 0.51214 | 0.51204 | 0.51244 | –7.64 | 1276 | 1568 |
| YP-4 | Quartz porphyry | 30.0169 | 0.78149 | 0.71236 | 0.0883 | 0.51196 | 0.51187 | 0.51243 | –10.95 | 1444 | 1840 |
| YP06-4 | Quartz porphyry | 7.1347 | 0.72241 | 0.70598 | 0.09 | 0.51212 | 0.51202 | 0.51243 | –7.92 | 1271 | 1595 |
| YP06-26 | Quartz porphyry | 9.8552 | 0.72671 | 0.70401 | 0.0934 | 0.51217 | 0.51207 | 0.51243 | –7.02 | 1244 | 1521 |
| YP06-18 | Quartz porphyry | 6.6835 | 0.72389 | 0.70849 | 0.0937 | 0.51217 | 0.51207 | 0.51243 | –6.94 | 1242 | 1516 |
| YP-9 | Granite porphyry | 4.4827 | 0.73155 | 0.70378 | 0.0976 | 0.51168 | 0.51140 | 0.51208 | –13.23 | 1929 | 2246 |

Notes:
(1) $(^{87}Sr/^{86}Sr)_i$ refer to the initial Sr isotopic ratios at time t; $^{87}Rb$ decay constant $\lambda = 1.42 \times 10^{-11}$ (Steiger & Jäger, 1977).
(2) $^{143}Nd/^{144}Nd(t)$ refer to the initial Nd isotopic ratios at time t; $^{147}Sm$ decay constant $\lambda = 6.54 \times 10^{-12}$ (Lugmair & Marti, 1978).
(3) $Nd_{CHUR(t)}$ is the $^{143}Nd/^{144}Nd$ isotope ratios of CHUR (chondritic reservoir) at time t; $^{143}Nd/^{144}Nd$(CHUR, Today) = 0.512638 (Goldstein *et al*., 1984), $^{147}Sm/^{144}Nd$(CHUR, Today) = 0.1967 (Peucat *et al*., 1989), (4) $T_{DM1}$ (Ma) refer to the single stage model age relative to depleted mantle (DM). DM: $^{147}Sm/^{144}Nd = 0.2137$, $^{143}Nd/^{144}Nd = 0.51315$ (Peucat *et al*., 1989)
(5) $T_{DM2}$ (Ma) refer to the two-stage model age relative to depleted mantle. Continental crustal: $^{147}Sm/^{144}Nd = 0.118$ (Jahn & Condie, 1995)
(6) t = 157 Ma is used for dacite porphyry (YP06-16, YP06-17, YP06-20, YP06-21), t = 162Ma is used for quartz porphyry (YP-4, YP06-4, YP06-26, YP06-18), and t = 435 Ma is used for granite porphyry (YP-9).

#### *5.3.2 Sample YP06-16*

A total of 15 spots were analyzed on 14 zircon grains selected from sample YP06-16 from the dacite porphyry. This sample yields a $^{206}Pb/^{238}U$ weighted average age of 157.5 ± 2.9 Ma ($n$ = 14 zircons, MSWD = 0.32). An inherited zircon crystal yields a Silurian age (~430 Ma) (Fig. 7b, Table 3).

#### *5.3.3 Sample YP06-17*

A total of 14 spots were analyzed on 14 zircon grains selected from sample YP06-17 from the dacite porphyry. This sample yields a weighted average age of 156.0 ± 3.1 Ma ($n$ = 12 zircons, MSWD = 0.19), although an inherited grain shows a Neo-Proterozoic age (~766 Ma). Another zircon grain gives a Late Cambrian age (~498 Ma) (Fig. 7c, Table 3).

#### *5.3.4 Sample YP06-18*

A total of 15 spots were analyzed on 15 zircon grains selected from sample YP06-18 which was collected from the quartz porphyry. This sample yields a weighted average age of 162.1 ± 3.4 Ma ($n$ = 10 zircons, MSWD = 0.35). Three grains (No. 2, No.9, and No.13) yield a weighted average age of 432 ± 16 Ma. A zircon with narrow growth zoning has a Late Triassic age (~208.6 Ma) and another one with narrow growth zoning shows an Early Jurassic age (Fig. 7d, Table 3).

### 5.4 Zircon Hf isotopes

A total of 65 spots of in-situ Hf isotope analysis were analyzed on zircon grains selected from samples dacite porphyry (YP06-16, YP06-17), and quartz porphyry (YP06-18). The results (Table 4) demonstrate negative initial $\varepsilon_{Hf}(t)$ values. The $\varepsilon_{Hf}(t)$ values of sample YP06-16 range from –17 to –5.6, mostly between –10 and –8, except for several spots that have negative initial $\varepsilon_{Hf}$ (t) values ranging from –19 to –13. The $\varepsilon_{Hf}$ (t) values of sample YP06-17 has a wider range between –20.0 and –4.9. The $\varepsilon_{Hf}$ (t) values of sample YP06-18 also has a wider range from –19.8 to –6.3 with two peaks at –18 to –16 and –10 to –8 (Table 4). The negative initial $\varepsilon_{Hf}(t)$ values could imply a crustal magma source, which is in good agreement with the Nd–Sr isotope compositions of the samples.

### 5.5 Biotite and muscovite Ar–Ar ages

The $^{40}Ar$–$^{39}Ar$ ages and 2σ uncertainties are plotted against the cumulative released $^{39}Ar$ fraction to establish step heating spectra (Fig. 8). The argon isotope ratios are presented graphically on classic isotope correlation plots using program ISOPLOT of Ludwig (2001). The $^{40}Ar$–$^{39}Ar$ data of biotite and muscovite are summarized in Tables 5–7, which incorporate the apparent age spectra and the atmospheric argon and Ca:K ratios for each step heating. The muscovite selected from quartz porphyry YP06-4 has a plateau

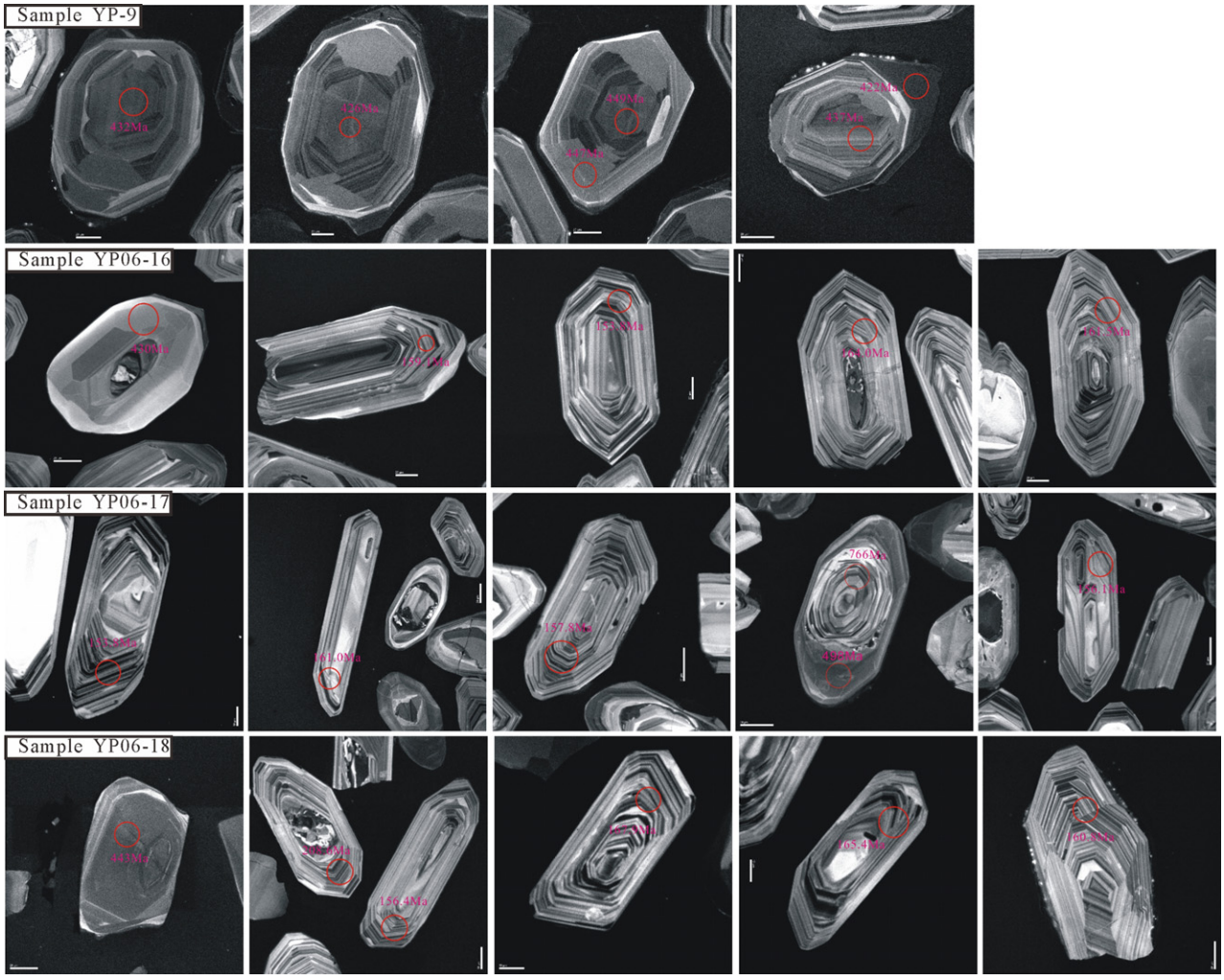


**Fig. 6** Cathodoluminescence images of zircons selected from samples granite porphyry (YP-9), dacite porphyry (YP06-116, YP06-17) and quartz porphyry (YP06-18). SHRIMP target spots are marked by circles and are approximately 25 μm in diameter. Cathodoluminescence images were acquired at the Institute of Mineral Resources, Chinese Academy of Geological Sciences, using a JOEL JXA 8800R, at 20 kV, 10 nA.

age of 162.1 ± 1.4 Ma, calculated from steps 5–11, representing 62.1% of the total argon release (Fig. 8a). The isochron age of 161 ± 4 Ma (MSWD = 0.106, initial $^{40}Ar/^{36}Ar$ = 318) is concordant with the plateau age (Fig. 8a).

The biotite selected from dacite porphyry (YP06-16, YP06-17) have plateau ages of 164 ± 1.3 Ma and 163.8 ± 1.3 Ma, both of which were calculated from steps 3–10, representing 95% and 95.1% of the total argon release, respectively. Both samples show similar isochron ages: sample YP06-16 of 164.8 ± 3.4 Ma (MSWD = 0.62) and sample YP06-17 of 164 ± 3 Ma (MSWD = 0.23) (Fig. 8b,c).

### 5.6 Molybdenite Re–Os results

Two Re–Os molybdenite analyses are reported in Table 8. The concentrations of total Re and $^{187}Os$ range in 19.25–79 ppm and in 32–130 ppb, respectively. The samples were analyzed only once because the ages of both samples (155.7 ± 3.6 Ma and 156 ± 2.8 Ma (2σ)) are nearly identical within the allowed error limit.

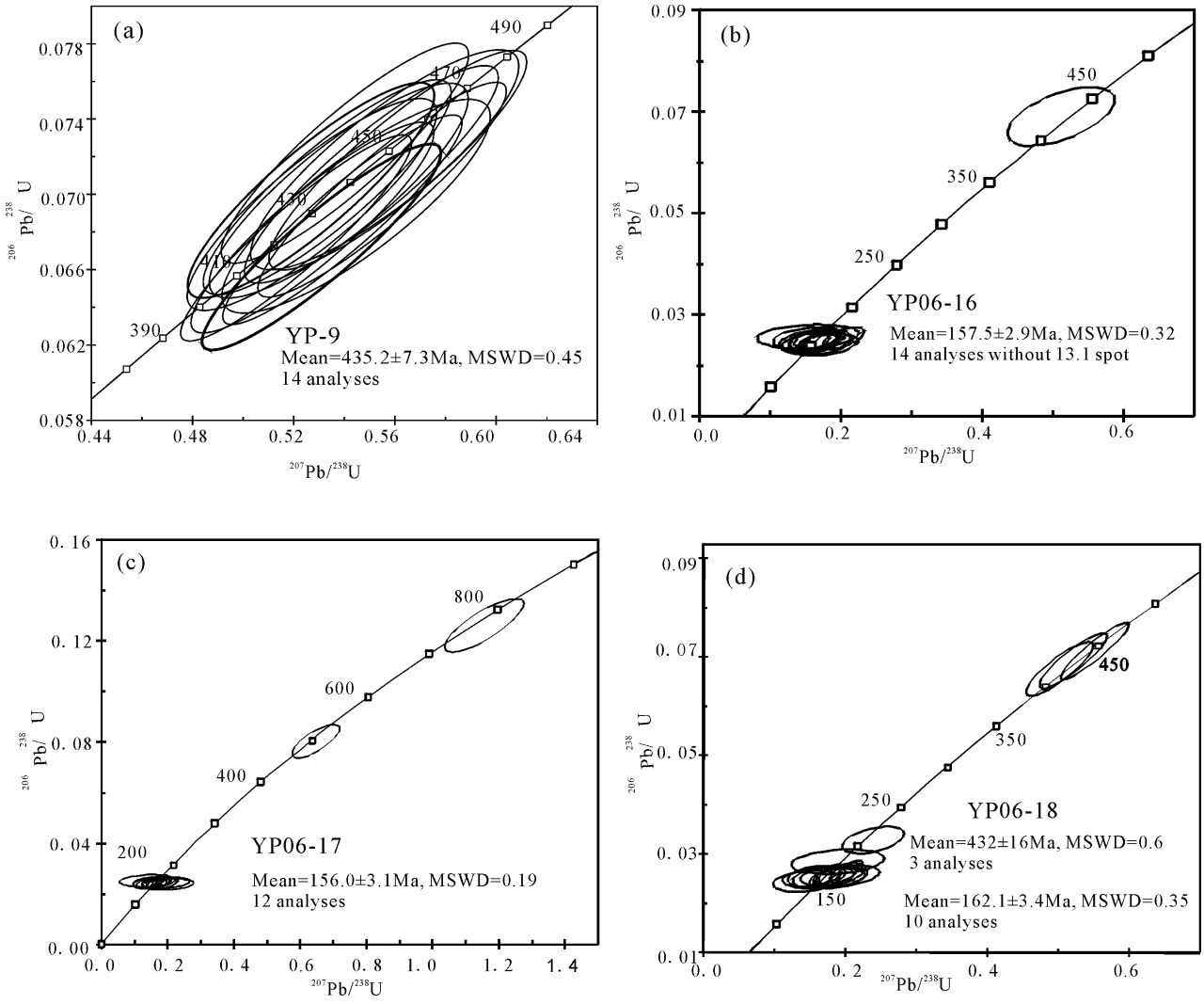


**Fig. 7** Concordia plot showing all SHRIMP data for zircons selected from granite porphyry (YP-9), dacite porphyry (YP06-16, YP06-17) and quartz porphyry (YP06-18).

## 6. Discussions

### 6.1 Zircon morphology and Th–U geochemistry

*6.1.1 Zircon morphology*

Cathodoluminescence images of the analyzed samples reveal that all the zircons from the Yongping deposit contain inherited cores surrounded by either magmatic or recrystallized rims (Fig. 6). The ages recorded in the inherited cores can be treated similarly to detrital crystals and used to fingerprint their source (Elburg, 1996).

Zircon recrystallized or overgrown during metamorphism could show high or low luminescence in CL images due to different redistribution of REE and U. Hydrothermal zircons may show spongy texture due to the presence of fluid-inclusions (Hoskin, 1998). The apparent systematic distinction between igneous zircons and metamorphic zircons is recongnized in the Th/U ratios, which is very low for the latter (<0.07; Rubatto, 2002). Igneous zircons generally have Th/U ratio equal to or greater than 0.5 (Hoskin & Schaltegger, 2003). Igneous zircons with low Th/U ratios (less than 0.5) may have crystallized in the presence of aqueous fluids (Bacon & Lowenstern, 2005).

**Table 3** Zircon SHRIMP U–Pb data for the igneous rocks in the Yongping copper deposit.

| Spots | Rock types | $\%^{206}Pb_c$ | U ppm | Th ppm | $^{232}Th/^{238}U$ | $^{206}Pb^*$ ppm | $^{207}Pb^*/^{206}Pb^*$ | ± % | $^{207}Pb^*/^{235}U$ | ± % | $^{206}Pb^*/^{238}U$ | ± % | errcorr | $^{206}Pb/^{238}U$ Age | | $^{207}Pb/^{206}Pb$ Age | | % Discordant |
|---|---|---|---|---|---|---|---|---|---|---|---|---|---|---|---|---|---|---|
| YP-9-1.1 | Granite | 0.25 | 1171 | 28 | 0.02 | 72.8 | 0.05428 | 1.7 | 0.540 | 3.7 | 0.0722 | 3.3 | .894 | 449 | ±14 | 383 | ±37 | –17 |
| YP-9-1.2 | porphyry | 0.12 | 892 | 20 | 0.02 | 55.1 | 0.05667 | 1.7 | 0.561 | 3.7 | 0.0718 | 3.3 | .895 | 447 | ±14 | 479 | ±37 | 7 |
| YP-9-2.1 | | 0.15 | 1142 | 27 | 0.02 | 67.1 | 0.05606 | 1.6 | 0.527 | 3.7 | 0.0682 | 3.3 | .901 | 426 | ±14 | 455 | ±36 | 6 |
| YP-9-3.1 | | 0.05 | 1331 | 24 | 0.02 | 76.9 | 0.05730 | 1.5 | 0.531 | 3.6 | 0.0672 | 3.3 | .915 | 419 | ±13 | 503 | ±32 | 17 |
| YP-9-4.1 | | 0.33 | 843 | 48 | 0.06 | 50.4 | 0.0569 | 2.2 | 0.545 | 4.0 | 0.0694 | 3.3 | .840 | 432 | ±14 | 490 | ±48 | 12 |
| YP-9-5.1 | | 0.33 | 839 | 19 | 0.02 | 52.0 | 0.0561 | 2.0 | 0.556 | 3.9 | 0.0718 | 3.3 | .853 | 447 | ±14 | 458 | ±45 | 2 |
| YP-9-6.1 | | 0.20 | 1164 | 28 | 0.02 | 71.2 | 0.05620 | 1.7 | 0.551 | 3.7 | 0.0711 | 3.3 | .893 | 443 | ±14 | 461 | ±37 | 4 |
| YP-9-7.1 | | 0.14 | 1213 | 28 | 0.02 | 71.7 | 0.05697 | 1.4 | 0.539 | 3.6 | 0.0687 | 3.3 | .924 | 428 | ±14 | 491 | ±30 | 13 |
| YP-9-8.1 | | 0.25 | 897 | 18 | 0.02 | 54.2 | 0.0556 | 2.0 | 0.538 | 3.9 | 0.0702 | 3.3 | .855 | 437 | ±14 | 435 | ±45 | –1 |
| YP-9-8.2 | | 0.13 | 1867 | 12 | 0.01 | 109 | 0.05582 | 1.4 | 0.521 | 3.6 | 0.0677 | 3.3 | .923 | 422 | ±13 | 445 | ±31 | 5 |
| YP-9-9.1 | | 0.14 | 986 | 18 | 0.02 | 59.6 | 0.05729 | 1.4 | 0.555 | 3.6 | 0.0703 | 3.3 | .918 | 438 | ±14 | 503 | ±32 | 13 |
| YP-9–10.1 | | 0.24 | 1097 | 19 | 0.02 | 66.3 | 0.05442 | 1.8 | 0.527 | 3.8 | 0.0702 | 3.3 | .880 | 438 | ±14 | 389 | ±40 | –13 |
| YP-9–11.1 | | 0.25 | 1112 | 15 | 0.01 | 67.4 | 0.05495 | 1.8 | 0.533 | 3.8 | 0.0704 | 3.3 | .882 | 439 | ±14 | 410 | ±40 | –7 |
| YP-9–12.1 | | 0.40 | 1234 | 28 | 0.02 | 73.9 | 0.0550 | 1.9 | 0.527 | 3.8 | 0.0695 | 3.3 | .866 | 433 | ±14 | 414 | ±43 | –4 |
| YP06-16-1.1 | Dacite | 1.71 | 694 | 176 | 0.26 | 15.1 | 0.0485 | 9.0 | 0.167 | 9.6 | 0.02499 | 3.4 | .356 | 159.1 | ±5.4 | 128 | ±210 | –24 |
| YP06-16-2.1 | porphyry | 0.52 | 518 | 86 | 0.17 | 11.3 | 0.0586 | 4.7 | 0.205 | 5.9 | 0.02536 | 3.5 | .591 | 161.5 | ±5.5 | 551 | ±100 | 71 |
| YP06-16-3.1 | | 1.52 | 482 | 101 | 0.22 | 10.4 | 0.0475 | 7.8 | 0.162 | 8.6 | 0.02466 | 3.5 | .409 | 157.1 | ±5.4 | 78 | ±190 | –102 |
| YP06-16-4.1 | | 0.86 | 634 | 140 | 0.23 | 13.3 | 0.0535 | 8.0 | 0.179 | 8.7 | 0.02431 | 3.5 | .398 | 154.9 | ±5.3 | 350 | ±180 | 56 |
| YP06-16-5.1 | | 1.23 | 767 | 207 | 0.28 | 16.1 | 0.0484 | 4.9 | 0.1613 | 6.0 | 0.02415 | 3.4 | .572 | 153.8 | ±5.2 | 121 | ±120 | –28 |
| YP06-16-6.1 | | 0.86 | 782 | 223 | 0.29 | 16.9 | 0.0511 | 4.8 | 0.176 | 5.9 | 0.02493 | 3.4 | .580 | 158.7 | ±5.3 | 248 | ±110 | 36 |
| YP06-16-7.1 | | 0.83 | 713 | 202 | 0.29 | 15.2 | 0.0502 | 5.0 | 0.170 | 6.1 | 0.02462 | 3.4 | .562 | 156.8 | ±5.3 | 205 | ±120 | 24 |
| YP06-16-8.1 | | 1.21 | 903 | 344 | 0.39 | 19.8 | 0.0482 | 6.9 | 0.168 | 7.7 | 0.02522 | 3.5 | .456 | 160.6 | ±5.6 | 109 | ±160 | –47 |
| YP06-16-9.1 | | 0.73 | 507 | 93 | 0.19 | 10.7 | 0.0537 | 6.5 | 0.180 | 7.7 | 0.02435 | 4.1 | .531 | 155.1 | ±6.2 | 361 | ±150 | 57 |
| YP06-16-10.1 | | 1.78 | 623 | 206 | 0.34 | 13.8 | 0.0438 | 12 | 0.153 | 12 | 0.02529 | 3.5 | .281 | 161.0 | ±5.5 | –120 | ±290 | 234 |
| YP06-16-11.1 | | 1.34 | 575 | 114 | 0.21 | 12.2 | 0.0471 | 9.9 | 0.158 | 10 | 0.02435 | 3.5 | .333 | 155.1 | ±5.3 | 56 | ±230 | –178 |
| YP06-16-12.1 | | 1.88 | 695 | 253 | 0.38 | 15.1 | 0.0467 | 11 | 0.160 | 11 | 0.02477 | 3.5 | .301 | 157.7 | ±5.4 | 38 | ±260 | –318 |
| YP06-16-13.1 | | 0.67 | 377 | 38 | 0.10 | 22.4 | 0.0539 | 5.0 | 0.513 | 6.0 | 0.0689 | 3.4 | .567 | 430 | ±14 | 369 | ±110 | –17 |
| YP06-16-14.1 | | 3.08 | 370 | 76 | 0.21 | 8.43 | 0.0438 | 19 | 0.156 | 19 | 0.02577 | 3.6 | .192 | 164.0 | ±5.9 | –119 | ±460 | 238 |
| YP06-16-14.2 | | 1.43 | 465 | 100 | 0.22 | 9.76 | 0.0548 | 9.0 | 0.183 | 9.6 | 0.02413 | 3.5 | .366 | 153.7 | ±5.3 | 407 | ±200 | 62 |

**Table 3** *Continued*

| Spots | Rock types | %$^{206}Pb_c$ | U ppm | Th ppm | $^{232}Th/^{238}U$ | $^{206}Pb^*$ ppm | $^{207}Pb^*/^{206}Pb^*$ | ± % | $^{207}Pb^*/^{235}U$ | ± % | $^{206}Pb^*/^{238}U$ | ± % | errcorr | $^{206}Pb/^{238}U$ Age | | $^{207}Pb/^{206}Pb$ Age | | % Discordant |
|---|---|---|---|---|---|---|---|---|---|---|---|---|---|---|---|---|---|---|
| YP06-17-1.1 | Dacite | 3.67 | 366 | 151 | 0.43 | 8.23 | 0.0405 | 24 | 0.141 | 24 | 0.0253 | 4.0 | .163 | 161.0 | ±6.3 | –314 | ±620 | 151 |
| YP06-17-2.1 | porphyry | 1.75 | 332 | 147 | 0.46 | 6.91 | 0.0618 | 15 | 0.203 | 15 | 0.0238 | 3.7 | .237 | 151.8 | ±5.5 | 668 | ±320 | 77 |
| YP06-17-3.1 | | 0.56 | 424 | 123 | 0.30 | 8.94 | 0.0594 | 5.2 | 0.200 | 6.3 | 0.0244 | 3.5 | .557 | 155.6 | ±5.4 | 581 | ±110 | 73 |
| YP06-17-4.1 | | 1.66 | 406 | 55 | 0.14 | 8.58 | 0.0455 | 12 | 0.152 | 12 | 0.0242 | 3.5 | .290 | 154.2 | ±5.4 | –24 | ±280 | 736 |
| YP06-17-5.1 | | 0.41 | 866 | 255 | 0.30 | 18.7 | 0.0465 | 5.1 | 0.1604 | 6.1 | 0.0250 | 3.4 | .557 | 159.4 | ±5.3 | 23 | ±120 | –584 |
| YP06-17-6.1 | | 0.84 | 451 | 112 | 0.26 | 9.68 | 0.0551 | 4.2 | 0.188 | 5.5 | 0.0247 | 3.5 | .634 | 157.8 | ±5.4 | 416 | ±95 | 62 |
| YP06-17-7.1 | | 1.58 | 591 | 163 | 0.28 | 12.6 | 0.0419 | 12 | 0.141 | 12 | 0.0244 | 3.5 | .288 | 155.3 | ±5.3 | –229 | ±290 | 168 |
| YP06-17-8.1 | | 2.36 | 389 | 85 | 0.23 | 8.37 | 0.0489 | 17 | 0.165 | 17 | 0.0245 | 4.1 | .241 | 155.9 | ±6.3 | 144 | ±390 | –8 |
| YP06-17-9.1 | | 0.31 | 654 | 132 | 0.21 | 13.9 | 0.0544 | 3.7 | 0.1852 | 5.0 | 0.0247 | 3.4 | .682 | 157.1 | ±5.3 | 389 | ±83 | 60 |
| YP06-17-10.1 | | 0.48 | 522 | 86 | 0.17 | 36.2 | 0.0586 | 3.0 | 0.649 | 4.5 | 0.0803 | 3.4 | .751 | 498 | ±16 | 551 | ±65 | 10 |
| YP06-17-11.1 | | 0.31 | 360 | 278 | 0.80 | 39.1 | 0.0666 | 2.5 | 1.157 | 4.2 | 0.1261 | 3.4 | .810 | 766 | ±25 | 824 | ±51 | 7 |
| YP06-17-12.1 | | 0.69 | 799 | 337 | 0.44 | 17.1 | 0.0504 | 3.4 | 0.1717 | 4.8 | 0.0247 | 3.4 | .702 | 157.3 | ±5.3 | 215 | ±80 | 27 |
| YP06-17-13.1 | | 0.62 | 686 | 174 | 0.26 | 14.3 | 0.0481 | 4.8 | 0.1603 | 5.9 | 0.0241 | 3.4 | .581 | 153.8 | ±5.2 | 107 | ±110 | –44 |
| YP06-17-14.1 | | 2.21 | 343 | 55 | 0.17 | 7.37 | 0.0581 | 15 | 0.196 | 15 | 0.0245 | 3.7 | .248 | 156.1 | ±5.7 | 534 | ±320 | 71 |
| YP06-18-1.1 | Quartz | 2.56 | 585 | 120 | 0.21 | 13.0 | 0.0487 | 14 | 0.170 | 14 | 0.02526 | 3.5 | .248 | 160.8 | ±5.5 | 136 | ±320 | –18 |
| YP06-18-2.1 | porphyry | 0.11 | 1328 | 7 | 0.01 | 81.3 | 0.05618 | 1.3 | 0.551 | 3.6 | 0.0712 | 3.3 | .929 | 443 | ±14 | 459 | ±29 | 4 |
| YP06-18-3.1 | | 1.33 | 410 | 94 | 0.24 | 9.14 | 0.0545 | 11 | 0.193 | 12 | 0.02562 | 3.5 | .297 | 163.1 | ±5.6 | 394 | ±250 | 59 |
| YP06-18-4.1 | | 1.39 | 604 | 128 | 0.22 | 13.3 | 0.0552 | 7.4 | 0.192 | 8.1 | 0.02526 | 3.4 | .424 | 160.8 | ±5.5 | 422 | ±160 | 62 |
| YP06-18-5.1 | | 2.03 | 643 | 258 | 0.41 | 13.8 | 0.0428 | 13 | 0.145 | 13 | 0.02456 | 3.6 | .278 | 156.4 | ±5.6 | –174 | ±310 | 190 |
| YP06-18-6.1 | | 1.19 | 696 | 138 | 0.21 | 19.9 | 0.0528 | 6.5 | 0.240 | 7.3 | 0.0329 | 3.4 | .464 | 208.6 | ±7.0 | 321 | ±150 | 35 |
| YP06-18-7.1 | | 0.83 | 978 | 416 | 0.44 | 21.3 | 0.0504 | 5.0 | 0.175 | 6.0 | 0.02515 | 3.4 | .562 | 160.1 | ±5.3 | 215 | ±120 | 25 |
| YP06-18-8.1 | | 1.44 | 757 | 190 | 0.26 | 16.8 | 0.0445 | 9.2 | 0.157 | 9.8 | 0.02551 | 3.4 | .348 | 162.4 | ±5.5 | –81 | ±220 | 301 |
| YP06-18-9.1 | | 0.28 | 1322 | 9 | 0.01 | 78.8 | 0.05457 | 1.7 | 0.521 | 3.7 | 0.0692 | 3.3 | .888 | 432 | ±14 | 395 | ±38 | –9 |
| YP06-18-10.1 | | 0.38 | 378 | 170 | 0.47 | 8.48 | 0.0545 | 5.9 | 0.195 | 6.8 | 0.02599 | 3.5 | .512 | 165.4 | ±5.7 | 393 | ±130 | 58 |
| YP06-18-11.1 | | 0.33 | 1520 | 525 | 0.36 | 33.9 | 0.0494 | 2.9 | 0.1764 | 4.4 | 0.02590 | 3.3 | .759 | 164.8 | ±5.4 | 166 | ±67 | 1 |
| YP06-18-12.1 | | 0.18 | 935 | 308 | 0.34 | 21.2 | 0.0552 | 3.3 | 0.2010 | 4.7 | 0.02640 | 3.4 | .722 | 167.9 | ±5.7 | 422 | ±73 | 60 |
| YP06-18-13.1 | | 0.25 | 1257 | 8 | 0.01 | 73.1 | 0.0539 | 1.9 | 0.502 | 3.8 | 0.0676 | 3.3 | .862 | 422 | ±14 | 367 | ±44 | –15 |
| YP06-18-14.1 | | 2.32 | 455 | 165 | 0.38 | 11.4 | 0.0483 | 14 | 0.190 | 14 | 0.0285 | 3.6 | .253 | 181.1 | ±6.4 | 115 | ±320 | –57 |
| YP06-18-15.1 | | 1.28 | 620 | 275 | 0.46 | 13.6 | 0.0485 | 9.8 | 0.169 | 10 | 0.02527 | 3.5 | .334 | 160.9 | ±5.5 | 123 | ±230 | –30 |

Errors are 1-sigma; $Pb_c$ and Pb* indicate the common and radiogenic portions, respectively.
Error in standard calibration was 1.09% (not included in above errors but required when comparing data from different mounts).
(1) Common Pb corrected using measured $^{204}Pb$.
(2) Common Pb corrected by assuming $^{206}Pb/^{238}U$-$^{207}Pb/^{235}U$ age-concordance.
(3) Common Pb corrected by assuming $^{206}Pb/^{238}U$-$^{208}Pb/^{232}Th$ age-concordance.

**Table 4** Zircon Hf isotopic compositions of the igneous rocks in the Yongping Cu–Mo deposits

| Samples | Rock types | $^{176}Hf/^{177}Hf$ | $^{176}Lu/^{177}Hf$ | t (Ga) | $\varepsilon_{Hf(t)}$ | $^{176}Hf/^{177}Hf_{(t)}$ | $T_{DM1}$(Ga) | $T_{DM2}$(Ga) |
|---|---|---|---|---|---|---|---|---|
| YP-9-0-1 | Granite | 0.28214 | 0.00032 | 0.44700 | –12.49112 | 0.28214 | 1.53395 | 2.21603 |
| YP-9-0-2 | porphyry | 0.28212 | 0.00031 | 0.42600 | –13.84187 | 0.28212 | 1.56816 | 2.28520 |
| YP-9-1-1 | | 0.28218 | 0.00036 | 0.42600 | –11.79173 | 0.28217 | 1.49046 | 2.15633 |
| YP-9-2-1 | | 0.28214 | 0.00020 | 0.44900 | –12.55429 | 0.28214 | 1.53494 | 2.22155 |
| YP-9-3-1 | | 0.28217 | 0.00018 | 0.41900 | –11.96696 | 0.28217 | 1.48638 | 2.16219 |
| YP-9-4-1 | | 0.28214 | 0.00015 | 0.43200 | –13.00868 | 0.28214 | 1.53645 | 2.23742 |
| YP-9-5-1 | | 0.28216 | 0.00024 | 0.44700 | –11.95050 | 0.28216 | 1.51100 | 2.18209 |
| YP-9-6-1 | | 0.28215 | 0.00033 | 0.43200 | –12.65387 | 0.28215 | 1.52793 | 2.21504 |
| YP-9-7-1 | | 0.28216 | 0.00047 | 0.43200 | –12.23746 | 0.28216 | 1.51590 | 2.18880 |
| YP-9-8-1 | | 0.28215 | 0.00024 | 0.44300 | –12.22301 | 0.28215 | 1.51800 | 2.19622 |
| YP-9-9-1 | | 0.28214 | 0.00024 | 0.42800 | –12.85725 | 0.28214 | 1.52992 | 2.22487 |
| YP-9–10-1 | | 0.28215 | 0.00038 | 0.43200 | –12.78282 | 0.28214 | 1.53424 | 2.22312 |
| YP-9–11-1 | | 0.28215 | 0.00032 | 0.43700 | –12.52259 | 0.28215 | 1.52694 | 2.21053 |
| YP-9–11-2 | | 0.28207 | 0.00281 | 0.42200 | –16.33418 | 0.28205 | 1.74667 | 2.43698 |
| YP-9–12-1 | | 0.28210 | 0.00036 | 0.43200 | –14.36641 | 0.28210 | 1.59484 | 2.32258 |
| YP-9–13-1 | | 0.28216 | 0.00031 | 0.43200 | –12.23516 | 0.28216 | 1.51115 | 2.18873 |
| YP-9–14-1 | | 0.28216 | 0.00037 | 0.43800 | –12.27860 | 0.28215 | 1.51968 | 2.19592 |
| YP-9–15-1 | | 0.28213 | 0.00024 | 0.43200 | –13.12238 | 0.28213 | 1.54351 | 2.24452 |
| YP-9–16-1 | | 0.28215 | 0.00045 | 0.43200 | –12.60155 | 0.28215 | 1.52935 | 2.21169 |
| YP-9–17-1 | | 0.28212 | 0.00026 | 0.43900 | –13.35427 | 0.28212 | 1.55873 | 2.26431 |
| YP-9–18-1 | | 0.28218 | 0.00044 | 0.43200 | –11.68882 | 0.28217 | 1.49370 | 2.15432 |
| YP-9–18-2 | | 0.28208 | 0.00037 | 0.43200 | –15.20907 | 0.28207 | 1.62787 | 2.37545 |
| YP-9–19-1 | | 0.28215 | 0.00023 | 0.43200 | –12.61627 | 0.28215 | 1.52371 | 2.21272 |
| YP-9–20-1 | | 0.28212 | 0.00021 | 0.43300 | –13.43547 | 0.28212 | 1.55545 | 2.26495 |
| YP-9–21-1 | | 0.28218 | 0.00014 | 0.43200 | –11.61205 | 0.28218 | 1.48247 | 2.14962 |
| YP-9–22-1 | | 0.28217 | 0.00030 | 0.43200 | –12.05431 | 0.28216 | 1.50392 | 2.17736 |
| YP-9–23-1 | | 0.28213 | 0.00020 | 0.43200 | –13.09539 | 0.28213 | 1.54129 | 2.24284 |
| YP-9–24-1 | | 0.28213 | 0.00042 | 0.43200 | –13.15291 | 0.28213 | 1.54977 | 2.24635 |
| YP-9–25-1 | | 0.28216 | 0.00024 | 0.43200 | –12.37039 | 0.28215 | 1.51448 | 2.19726 |
| YP06-16-1-1 | Dacite | 0.28245 | 0.00054 | 0.15900 | –8.05539 | 0.28245 | 1.12382 | 1.72012 |
| YP06-16-1–2 | porphyry | 0.28245 | 0.00029 | 0.16200 | –7.84218 | 0.28245 | 1.11183 | 1.70896 |
| YP06-16-3-1 | | 0.28236 | 0.00035 | 0.15700 | –11.0682 | 0.28236 | 1.23459 | 1.90940 |
| YP06-16-4-1 | | 0.28251 | 0.00035 | 0.15700 | –6.00981 | 0.28250 | 1.03768 | 1.58897 |
| YP06-16-5-1 | | 0.28245 | 0.00046 | 0.15400 | –7.94990 | 0.28245 | 1.11356 | 1.70971 |
| YP06-16-6-1 | | 0.28248 | 0.00040 | 0.15900 | –7.02115 | 0.28247 | 1.07992 | 1.65461 |
| YP06-16-7-1 | | 0.28245 | 0.00048 | 0.15700 | –7.99673 | 0.28245 | 1.11838 | 1.71492 |
| YP06-16-8-1 | | 0.28240 | 0.00041 | 0.16100 | –9.78692 | 0.28240 | 1.18986 | 1.83131 |
| YP06-16-9-1 | | 0.28246 | 0.00040 | 0.15700 | –7.65614 | 0.28246 | 1.10303 | 1.69337 |
| YP06-16-10-1 | | 0.28246 | 0.00042 | 0.16100 | –7.55635 | 0.28246 | 1.10300 | 1.69004 |
| YP06-16-11-1 | | 0.28247 | 0.00037 | 0.15500 | –7.21093 | 0.28247 | 1.08326 | 1.66365 |
| YP06-16-12-1 | | 0.28245 | 0.00026 | 0.15500 | –7.93181 | 0.28245 | 1.10871 | 1.70938 |
| YP06-16-13-1 | | 0.28197 | 0.00086 | 0.43000 | –19.16091 | 0.28196 | 1.79600 | 2.62115 |
| YP06-16-14-1 | | 0.28241 | 0.00049 | 0.15800 | –9.28470 | 0.28241 | 1.16974 | 1.79724 |
| YP06-16-15-1 | | 0.28252 | 0.00041 | 0.16400 | –5.28074 | 0.28252 | 1.01644 | 1.54795 |
| YP06-16-16-1 | | 0.28247 | 0.00039 | 0.15700 | –7.23301 | 0.28247 | 1.08635 | 1.66654 |
| YP06-16-17-1 | | 0.28247 | 0.00029 | 0.15700 | –7.10046 | 0.28247 | 1.07868 | 1.65818 |
| YP06-16-18-1 | | 0.28212 | 0.00006 | 0.43000 | –13.49145 | 0.28212 | 1.55083 | 2.26630 |
| YP06-16-19-1 | | 0.28240 | 0.00038 | 0.15700 | –9.74901 | 0.28240 | 1.18411 | 1.82593 |
| YP06-16-20-1 | | 0.28242 | 0.00048 | 0.15700 | –9.20032 | 0.28241 | 1.16529 | 1.79116 |
| YP06-16-21-1 | | 0.28238 | 0.00104 | 0.15700 | –10.59943 | 0.28237 | 1.23596 | 1.87943 |
| YP06-16-22-1 | | 0.28241 | 0.00056 | 0.15700 | –9.27837 | 0.28241 | 1.17049 | 1.79607 |
| YP06-16-23-1 | | 0.28252 | 0.00064 | 0.15700 | –5.55713 | 0.28252 | 1.02660 | 1.56015 |
| YP06-16-24-1 | | 0.28219 | 0.00138 | 0.15700 | –17.12852 | 0.28219 | 1.50602 | 2.29101 |
| YP06-16-25-1 | | 0.28228 | 0.00031 | 0.15700 | –14.03855 | 0.28228 | 1.34890 | 2.09702 |

**Table 4** *Continued*

| Samples | Rock types | $^{176}Hf/^{177}Hf$ | $^{176}Lu/^{177}Hf$ | t (Ga) | $\varepsilon_{Hf(t)}$ | $^{176}Hf/^{177}Hf_{(t)}$ | $T_{DM1}$(Ga) | $T_{DM2}$(Ga) |
|---|---|---|---|---|---|---|---|---|
| YP06-17-2-1 | Dacite | 0.28236 | 0.00046 | 0.15200 | −11.11120 | 0.28236 | 1.23525 | 1.90832 |
| YP06-17-3-1 | porphyry | 0.28239 | 0.00050 | 0.15700 | −10.23911 | 0.28239 | 1.20640 | 1.85689 |
| YP06-17-5-1 | | 0.28220 | 0.00031 | 0.15700 | −16.66223 | 0.28220 | 1.45032 | 2.26241 |
| YP06-17-6-1 | | 0.28232 | 0.00050 | 0.15900 | −12.52401 | 0.28232 | 1.29732 | 2.00281 |
| YP06-17-7-1 | | 0.28250 | 0.00046 | 0.15700 | −6.11163 | 0.28250 | 1.04414 | 1.59539 |
| YP06-17-8-1 | | 0.28250 | 0.00055 | 0.15400 | −6.15630 | 0.28250 | 1.04545 | 1.59594 |
| YP06-17-9-1 | | 0.28223 | 0.00046 | 0.15900 | −15.63151 | 0.28223 | 1.41717 | 2.19886 |
| YP06-17-10-1 | | 0.28247 | 0.00041 | 0.15600 | −7.17436 | 0.28247 | 1.08358 | 1.66207 |
| YP06-17-11-1 | | 0.28254 | 0.00054 | 0.15700 | −4.90944 | 0.28254 | 0.99886 | 1.51905 |
| YP06-17-12-1 | | 0.28213 | 0.00059 | 0.76600 | −6.05133 | 0.28212 | 1.56155 | 2.05145 |
| YP06-17-12-2 | | 0.28210 | 0.00034 | 0.49800 | −13.01315 | 0.28209 | 1.59798 | 2.28693 |
| YP06-17-13-1 | | 0.28238 | 0.00040 | 0.15300 | −10.39933 | 0.28238 | 1.20678 | 1.86407 |
| YP06-17-14-1 | | 0.28209 | 0.00077 | 0.49800 | −13.51981 | 0.28208 | 1.63004 | 2.31850 |
| YP06-17-15-1 | | 0.28239 | 0.00057 | 0.15700 | −10.00960 | 0.28239 | 1.19956 | 1.84234 |
| YP06-17-16-1 | | 0.28213 | 0.00057 | 0.15700 | −19.14853 | 0.28213 | 1.55608 | 2.41864 |
| YP06-17-17-1 | | 0.28246 | 0.00072 | 0.15700 | −7.78764 | 0.28245 | 1.11617 | 1.70159 |
| YP06-17-18-1 | | 0.28211 | 0.00102 | 0.15700 | −20.04548 | 0.28211 | 1.60792 | 2.47462 |
| YP06-18-1-1 | Quartz | 0.28240 | 0.00034 | 0.16100 | −9.52294 | 0.28240 | 1.17765 | 1.81464 |
| YP06-18-2-1 | porphyry | 0.28195 | 0.00101 | 0.43300 | −19.83452 | 0.28194 | 1.83000 | 2.66537 |
| YP06-18-3-1 | | 0.28226 | 0.00078 | 0.16200 | −14.60124 | 0.28226 | 1.38995 | 2.13596 |
| YP06-18-4-1 | | 0.28220 | 0.00051 | 0.16200 | −16.77208 | 0.28220 | 1.46560 | 2.27290 |
| YP06-18-5-1 | | 0.28218 | 0.00111 | 0.16200 | −17.38215 | 0.28218 | 1.51048 | 2.31087 |
| YP06-18-6-1 | | 0.28218 | 0.00089 | 0.16200 | −17.47156 | 0.28218 | 1.50623 | 2.31665 |
| YP06-18-7-1 | | 0.28219 | 0.00064 | 0.16200 | −17.22961 | 0.28218 | 1.48805 | 2.30161 |
| YP06-18-8-1 | | 0.28226 | 0.00092 | 0.16200 | −14.81269 | 0.28225 | 1.40270 | 2.14921 |
| YP06-18-9-1 | | 0.28241 | 0.00057 | 0.16200 | −9.33715 | 0.28241 | 1.17743 | 1.80353 |
| YP06-18-10-1 | | 0.28243 | 0.00033 | 0.16100 | −8.66848 | 0.28243 | 1.14419 | 1.76054 |
| YP06-18-11-1 | | 0.28245 | 0.00051 | 0.15600 | −8.11085 | 0.28245 | 1.12266 | 1.72139 |
| YP06-18-12-1 | | 0.28247 | 0.00063 | 0.20900 | −6.25648 | 0.28247 | 1.09779 | 1.64373 |
| YP06-18-13-1 | | 0.28219 | 0.00101 | 0.16200 | −17.11019 | 0.28219 | 1.49629 | 2.29383 |
| YP06-18-14-1 | | 0.28219 | 0.00094 | 0.16200 | −17.17023 | 0.28219 | 1.49618 | 2.29766 |
| YP06-18-15-1 | | 0.28219 | 0.00083 | 0.16200 | −17.19565 | 0.28219 | 1.49326 | 2.29934 |
| YP06-18-16-1 | | 0.28223 | 0.00103 | 0.43200 | −9.96382 | 0.28222 | 1.44244 | 2.04553 |
| YP06-18-17-1 | | 0.28241 | 0.00078 | 0.16200 | −9.32460 | 0.28241 | 1.18263 | 1.80265 |
| YP06-18-18-1 | | 0.28224 | 0.00085 | 0.16200 | −15.19702 | 0.28224 | 1.41535 | 2.17348 |
| YP06-18-19-1 | | 0.28214 | 0.00081 | 0.16200 | −18.90690 | 0.28214 | 1.55944 | 2.40697 |
| YP06-18-20-1 | | 0.28217 | 0.00076 | 0.16200 | −17.90786 | 0.28217 | 1.51865 | 2.34419 |
| YP06-18-21-1 | | 0.28214 | 0.00080 | 0.16200 | −18.96232 | 0.28214 | 1.56126 | 2.41046 |

Note: t (Ma) refers to the time of single zircon grain formation. The single grains zircon SHRIMP U-Pb age was used to represent it.

The inherited cores of the zircon, in the porphyries can be grouped into three types: Type-1 are fragments or cores with well-defined concentric oscillatory zoning (Fig. 6, YP06-17-4); Type-2 are rounded, high luminescent cores with thin faint concentric zoning (Fig. 6, YP-9 and YP06-18-1); and Type-3 are also rounded, high luminescent cores without intra-grain structure (YP06-16-1). The surrounding rims can be grouped into: (i) rims characterized by well-defined concentric and oscillatory zoning, which is interpreted as magmatic overgrowth (YP06-16, YP06-17, and YP06-18); and (ii) nebulous, high-luminescent grains with structureless dark rims, suggesting a metamorphic recrystallization (YP-9).

### *6.1.2 Zircon Th–U chemistry*

The Th and U concentrations of zircon grains selected from four samples as the result of SHRIMP analysis are shown in Figures 9 and 10.

The Th/U ratios of zircon from dacite porphyry (YP06-17) range from 0.14 to 0.46 expect for the zircon grain No.10. The CL image of the zircon grain No.10 shows typical igneous characteristics in the core and

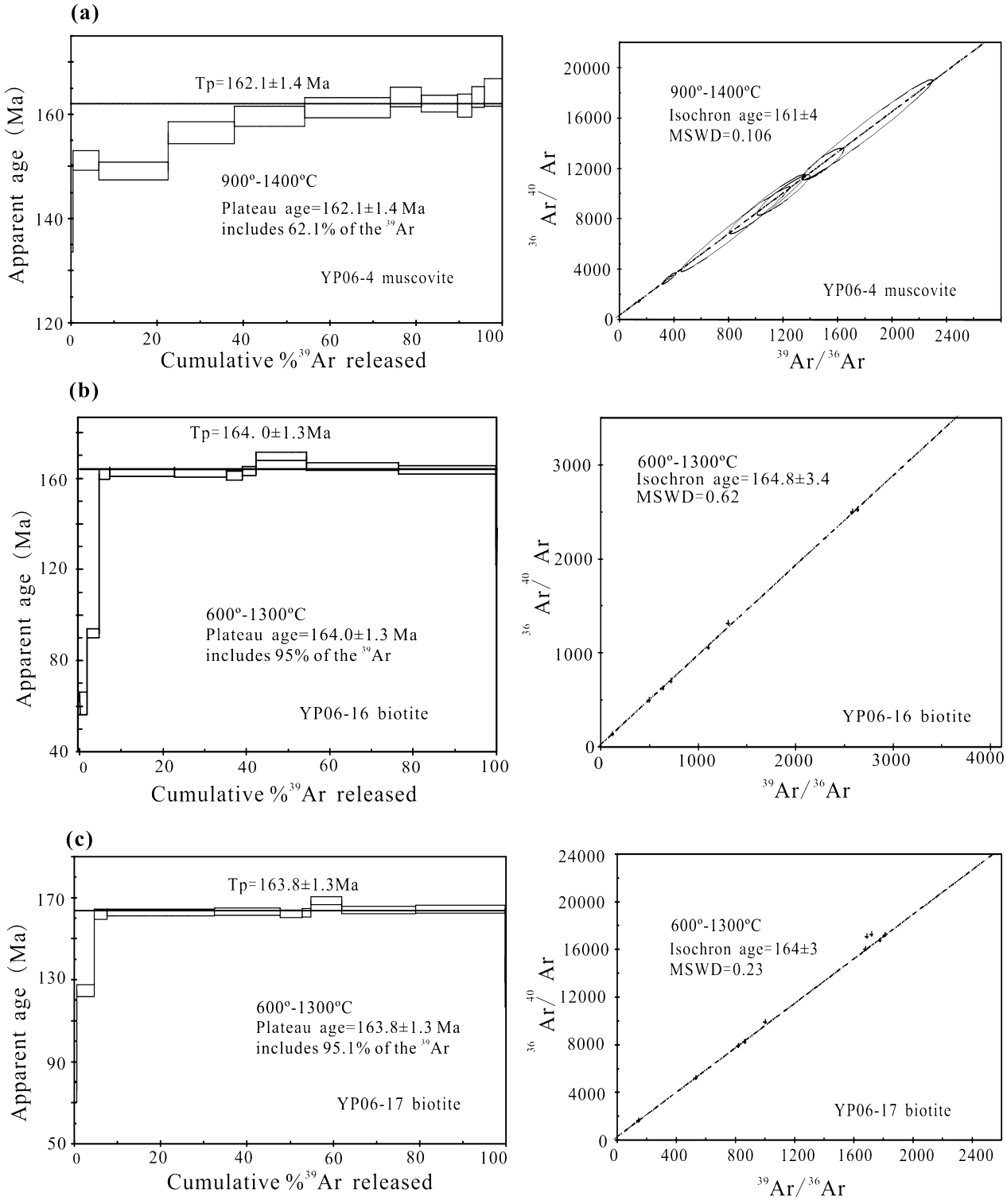


**Fig. 8** $^{40}Ar/^{39}Ar$ plateau ages and isochron ages of biotite and muscovite selected from dacite porphyry (YP06-16, YP06-17), and quartz porphyry (YP06-18).

**Table 5** Muscovite $^{40}Ar/^{36}Ar$ stepwise heating data of the altered quartz porphyry (YP06-4)

| T(°C) | $(^{40}Ar/^{39}Ar)_m$ | $(^{36}Ar/^{39}Ar)_m$ | $(^{37}Ar/^{39}Ar)_m$ | $(^{38}Ar/^{39}Ar)_m$ | $^{40}Ar^*/^{39}Ar$ | $^{39}Ar$ ($\times10^{-14}$mol) | $^{39}Ar$ (Cum.) (%) | Age (Ma) | Ca/K | ± 1σ (Ma) |
|---|---|---|---|---|---|---|---|---|---|---|
| 500 | 9.7748 | 0.0092 | 0.3048 | 0.0207 | 7.0725 | 20.27 | 0.49 | 142.0 | 0.32 | 8.4 |
| 600 | 8.2012 | 0.0022 | 0.0916 | 0.0145 | 7.5536 | 250.36 | 6.49 | 151.2 | 0.2918 | 1.9 |
| 700 | 7.6441 | 0.0007 | 0.0373 | 0.0128 | 7.4416 | 672.72 | 22.61 | 149.1 | 0.1959 | 1.7 |
| 800 | 7.9930 | 0.0006 | 0.0979 | 0.0127 | 7.8263 | 638.83 | 37.93 | 156.5 | 0.0901 | 2.1 |
| 900 | 8.2396 | 0.0009 | 0.1094 | 0.0128 | 7.9899 | 681.60 | 54.27 | 159.6 | 0.0472 | 1.9 |
| 1000 | 8.2818 | 0.0007 | 0.0215 | 0.0126 | 8.0793 | 825.97 | 74.07 | 161.3 | 0.0213 | 1.9 |
| 1050 | 8.4606 | 0.0009 | 0.0374 | 0.0129 | 8.1836 | 302.23 | 81.31 | 163.3 | 0.0661 | 1.9 |
| 1100 | 8.2864 | 0.0006 | 0.0688 | 0.0130 | 8.1197 | 346.39 | 89.61 | 162.1 | 0.0436 | 1.6 |
| 1200 | 8.4541 | 0.0012 | 0.1314 | 0.0138 | 8.1029 | 138.74 | 92.94 | 161.7 | 0.0421 | 2.2 |
| 1300 | 8.9950 | 0.0027 | 0.0648 | 0.0140 | 8.1833 | 123.16 | 95.89 | 163.3 | 0.0469 | 2.0 |
| 1400 | 10.2800 | 0.0070 | 0.1240 | 0.0141 | 8.2292 | 171.36 | 100.00 | 164.2 | 0.0066 | 2.6 |

W = 17.24 mg J = 0.011576.
Total age = 158.0 Ma.
F = $^{40}Ar^*/^{39}Ar$ (radiogenic).

**Table 6** Biotite $^{40}Ar/^{36}Ar$ stepwise heating data of the altered dacite porphyry (YP06-16)

| T(°C) | $(^{40}Ar/^{39}Ar)_m$ | $(^{36}Ar/^{39}Ar)_m$ | $(^{37}Ar/^{39}Ar)_m$ | $(^{38}Ar/^{39}Ar)_m$ | $^{40}Ar^*/^{39}Ar$ | $^{39}Ar$ ($\times10^{-14}$mol) | $^{39}Ar$ (Cum.) (%) | Age (Ma) | Ca/K | ± 1σ (Ma) |
|---|---|---|---|---|---|---|---|---|---|---|
| 400 | 12.6635 | 0.0312 | 0.1565 | 0.0232 | 27.20 | 144.39 | 1.68 | 61.4 | 61.4 | 5.0 |
| 500 | 9.8359 | 0.0157 | 0.2933 | 0.0220 | 53.00 | 255.72 | 4.64 | 92.1 | 92.1 | 2.0 |
| 600 | 11.8281 | 0.0084 | 0.0420 | 0.0206 | 79.12 | 221.25 | 7.21 | 162.1 | 162.1 | 2.3 |
| 700 | 9.8851 | 0.0016 | 0.0102 | 0.0158 | 95.25 | 1329.45 | 22.64 | 163.0 | 163.0 | 2.0 |
| 800 | 9.6477 | 0.0009 | 0.0144 | 0.0164 | 97.17 | 1086.34 | 35.25 | 162.4 | 162.4 | 1.7 |
| 900 | 9.7389 | 0.0014 | 0.0267 | 0.0188 | 95.73 | 318.46 | 38.95 | 161.5 | 161.5 | 2.0 |
| 1000 | 10.0394 | 0.0020 | 0.0331 | 0.0183 | 94.02 | 283.92 | 42.24 | 163.4 | 163.4 | 2.0 |
| 1100 | 10.0554 | 0.0008 | 0.0073 | 0.0144 | 97.71 | 1046.48 | 54.39 | 169.8 | 169.8 | 1.9 |
| 1200 | 9.6703 | 0.0004 | 0.0073 | 0.0143 | 98.77 | 1893.80 | 76.37 | 165.3 | 165.3 | 1.7 |
| 1300 | 9.5773 | 0.0004 | 0.0180 | 0.0143 | 98.78 | 2006.25 | 99.66 | 163.8 | 163.8 | 1.8 |
| 1400 | 9.9222 | 0.0084 | 0.3187 | 0.0346 | 75.05 | 29.46 | 100.00 | 130.2 | 130.2 | 8.0 |

W = 45.19 mg J = 0.010046.
Total age = 160.5 Ma.
F = $^{40}Ar^*/^{39}Ar$ (radiogenic).

**Table 7** Biotite $^{40}Ar/^{36}Ar$ stepwise heating data of the altered dacite porphyry (YP06-17)

| T(°C) | $(^{40}Ar/^{39}Ar)_m$ | $(^{36}Ar/^{39}Ar)_m$ | $(^{37}Ar/^{39}Ar)_m$ | $(^{38}Ar/^{39}Ar)_m$ | $^{40}Ar^*/^{39}Ar$ | $^{39}Ar$ ($\times10^{-14}$mol) | $^{39}Ar$ (Cum.) (%) | Age (Ma) | Ca/K | ± 1σ (Ma) |
|---|---|---|---|---|---|---|---|---|---|---|
| 400 | 15.0564 | 0.0368 | 0.2068 | 0.0279 | 27.82 | 52.46 | 0.60 | 75.5 | 75.5 | 5.2 |
| 500 | 13.2957 | 0.0213 | 0.1260 | 0.0235 | 52.71 | 359.45 | 4.68 | 124.6 | 124.6 | 2.7 |
| 600 | 11.2670 | 0.0069 | 0.0234 | 0.0168 | 81.77 | 265.07 | 7.68 | 162.1 | 162.1 | 2.5 |
| 700 | 9.6241 | 0.0012 | 0.0075 | 0.0146 | 96.20 | 2183.44 | 32.47 | 162.9 | 162.9 | 1.7 |
| 800 | 9.4547 | 0.0007 | 0.0101 | 0.0154 | 98.19 | 1341.63 | 47.70 | 163.3 | 163.3 | 1.8 |
| 900 | 9.5649 | 0.0012 | 0.0166 | 0.0160 | 96.37 | 455.01 | 52.86 | 162.2 | 162.2 | 1.8 |
| 1000 | 9.8096 | 0.0019 | 0.0300 | 0.0184 | 94.28 | 178.07 | 54.88 | 162.7 | 162.7 | 2.1 |
| 1100 | 9.9022 | 0.0010 | 0.0102 | 0.0151 | 96.97 | 622.38 | 61.95 | 168.6 | 168.6 | 2.0 |
| 1200 | 9.4998 | 0.0006 | 0.0081 | 0.0146 | 98.23 | 1514.17 | 79.14 | 164.1 | 164.1 | 1.7 |
| 1300 | 9.5381 | 0.0006 | 0.0263 | 0.0152 | 98.11 | 1822.16 | 99.82 | 164.5 | 164.5 | 1.9 |
| 1400 | 9.8520 | 0.0089 | 0.2421 | 0.0349 | 73.46 | 15.91 | 100.00 | 129 | 129 | 12 |

W = 45 mg J = 0.010205.
Total age = 161.7 Ma.
F = $^{40}Ar^*/^{39}Ar$ (radiogenic).

**Table 8** Molybdenite Re–Os geochronologic data

| Sample | Weight(g) | Re (μg $g^{-1}$) | $^{187}$Re (μg $g^{-1}$) | $^{187}$Os (ng $g^{-1}$) | Age (Ma) |
|---|---|---|---|---|---|
| YP-2 | 0.00740 | 79.351 ± 1.649 | 49.877 ± 1.037 | 129.57 ± 0.97 | 155.7 ± 3.6 |
| YP-10 | 0.01072 | 19.251 ± 0.243 | 12.101 ± 0.010 | 31.63 ± 0.32 | 156.7 ± 2.8 |

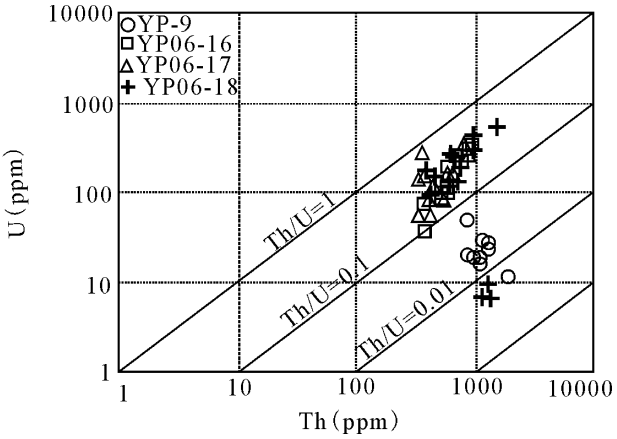


**Fig. 9** Diagram showing U and Th concentrations for granite porphyry (YP-9), dacite porphyry (YP06-116, YP06-17) and quartz porphyry (YP06-18).

metamorphic characteristics in the rim. The Th/U ratio is 0.17 for the rim and 0.80 for the core, which is similar to the results of Bacon & Lowenstern, (2005), and Hoskin and Schaltegger (2003). The Th/U ratio of zircon from dacite porphyry (YP06-16) ranges from 0.17 to 0.39 expect for the spot 13.1 which has a Th/U ratio of 0.1. The spots no. 2.1, no. 9.1, and no. 13.1 in zircon selected from quartz porphyry (YP06-18) show a constant Th/U ratio of 0.01, which is typical of a metamorphic origin, while the other spots in the same zircon show a Th/U ratio ranging from 0.21 to 0.47, which is typical of igneous origin. The spots in the zircon selected from the granite porphyry sample (YP-9) have a constant Th/U ratio of 0.02, except for the spots no. 4.1 (Th/U = 0.06), no. 8.2 (Th/U = 0.01), and no. 11.1 (Th/U = 0.01) (Fig. 9).

In order to discriminate the origin of zircons, this paper compares zircon ages with its Th/U ratios. As shown in Figure 10, the Th/U ratios of the zircons selected from samples YP06-16, YP06-17, and YP06-18 have wide Th/U ranges with constant ages, whereas sample YP-9 yields constant Th/U ratios and a narrow age range. It is proposed that the samples of YP06-16, YP06-17, and YP06-18 were probably derived from a mixed two sources, one with higher Th/U ratio and the other with lower Th/U ratio. Both sources could be either metamorphic or igneous. Sample YP-9, however, certainly has a metamorphic origin.

## 6.2 Interpretation of U–Pb, Ar–Ar and Re–Os ages

Previously published geochronological data for the Yongping deposit are mainly based on K–Ar and Rb–Sr analyses, and show a wide range of ages with large errors. The new U–Pb, Ar–Ar, and Re–Os molybdenite ages reported in this paper provide a better constraint on the timing of the magmatism and mineralization in the deposit. Zircons in granite porphyry (YP-9) have typical metamorphic characteristics based on their morphology and Th/U ratios. The sample yields a $^{206}$Pb/$^{238}$U weighted average age of 435.2 ± 7.3 Ma, suggesting an earlier Silurian metamorphic event. However, zircons in quartz porphyry (YP06-18) have typical igneous characteristics and show a weighted average age of 162.1 ± 3.4 Ma, suggesting a magmatic crystallization age for the quartz porphyry that is associated with the molybdenite mineralization of the Middle–Late Jurassic time. Sample YP06-18 yield two inherited zircons with ages of 432 ± 16 Ma and 208.6 ± 7 Ma, suggesting two metamorphic events prior to the intrusion and mineralization at the Yongping deposit.

Zircons in sample YP06-17 and YP06-16 collected from the dacite porphyries have typical igneous characteristics based on their morphology and Th/U ratios, and yield ages of 157.5 ± 2.9 Ma and 156.0 ± 1.3 Ma, respectively. The near-identical ages represent magmatic crystallization age for the dacite porphyry associated with copper mineralization in the Late Jurassic. Two inherited, metamorphic zircons yield ages of 498 ± 16 Ma and 430 ± 14 Ma, also suggesting two metamorphic events prior to the intrusion and mineralization at the deposit. The inherited age (766 ± 25 Ma) from a typical igneous zircon (with oscillatory zoning and Th/U = 0.8) may indicate a Neo-Proterozoic magmatic activity.

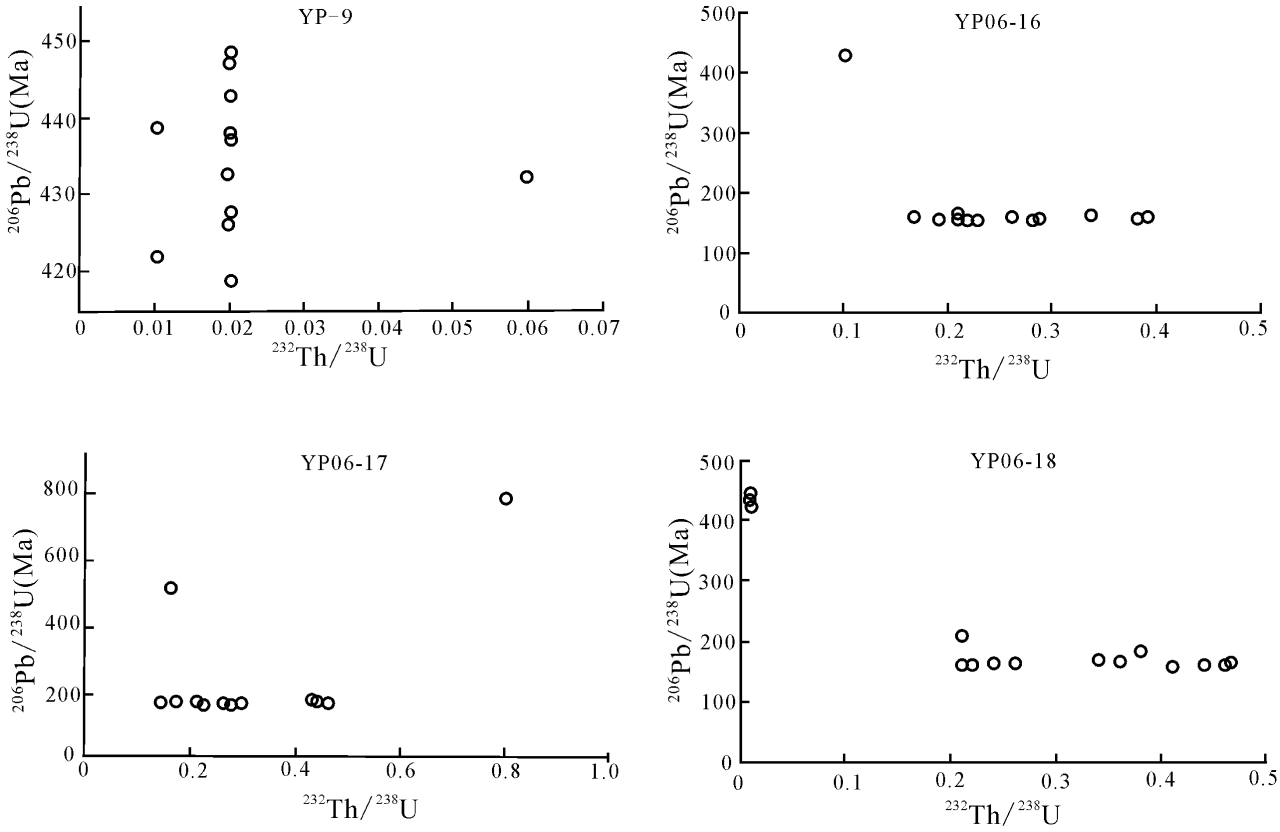


**Fig. 10** Diagram showing 206 Pb/238 U (Ma) and 232 Th/238 U ratios for granite porphyry (YP-9), dacite porphyry (YP06-116, YP06-17) and quartz porphyry (YP06-18).

Ar–Ar ages for hydrothermal biotite from the dacitie porphyry that is associated with copper mineralization and Ar–Ar ages for muscovite from the quartz porphyry that is associated with molybdenum suggest that, the muscovite crystallized later than the hydrothermal biotite. Two near-identical molybdenite Re–Os dating results, 155.7 ± 3.6 Ma and 156.7 ± 2.8 Ma, show a Late-Jurassic molybdenite crystallization subsequent to emplacement of the dacite porphyry.

Based on the zircon U–Pb age data, several episodes of magmatic and metamorphic events occurred in the deposit and its vicinities. The oldest magmatic activity in the deposit occurred in the Neo-Proterozoic time (766 ± 25 Ma), followed by Late Cambrian, Early Silurian, and Late Triassic metamorphic events. The Late Cambrian and Late Triassic events very likely caused migmatization. The Middle–Late Jurassic igneous event produced the dacite and quartz porphyries that were associated with the copper and molybdenum mineralization in the deposit.

### 6.3 Source of the magmas

Sr–Nd isotopes and zircon Hf isotopes of granitoids are a valuable tracer for magma sources. The quartz porphyry in the deposit has wide $\varepsilon_{Hf}$ (t) values of –6.2 to –18.9, and wide $\varepsilon_{Nd}$(t) values of –10.95 to –6.94. The dacite porphyry has wide $\varepsilon_{Hf}$ (t) values of –5.3 to –13.5, but narrow $\varepsilon_{Nd}$(t) values of –9.18 to –7.64. Their $\varepsilon_{Nd}$(t) values are close to that of the granites of southeast China (with $\varepsilon_{Nd}$(t) values from –16.4 to –1.1 and $I_{Sr}$ values from 0.7056 to 0.7404) (Shen *et al.*, 1998). The $\varepsilon_{Nd}$ (t) values represent the initial values of $\varepsilon_{Nd}$ in the rock at the time of its crystallization. The negative $\varepsilon_{Nd}$ (t) value implies a magma source with lower Sm/Nd than CHUR, i.e. enriched mantle sources or crustal source. The Sr–Nd isotopic data at Yongping suggests a dominated crustal source for both the dacite porphyry and the quartz porphyry. In the diagram of $\varepsilon_{Hf}$ (t)-t (Ma) (Fig. 11), the data plot in the intermediate area between depleted mantle and crust, also indicating a mixed magma source. In the $\varepsilon_{Nd}$ (t)-$I_{Sr}$ diagram (Fig. 12), all the

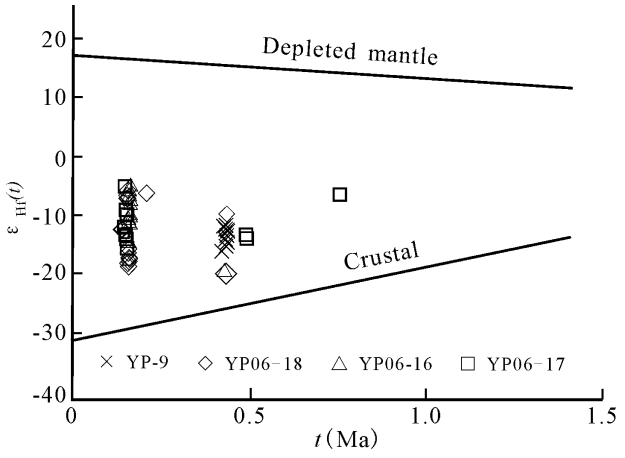


**Fig. 11** εHf (t)-t(Ma) diagram for granite porphyry (YP-9), dacite porphyry (YP06-116, YP06-17) and quartz porphyry (YP06-18). Depleted mantle and Crustal line are according to Shen *et al*. (1998).

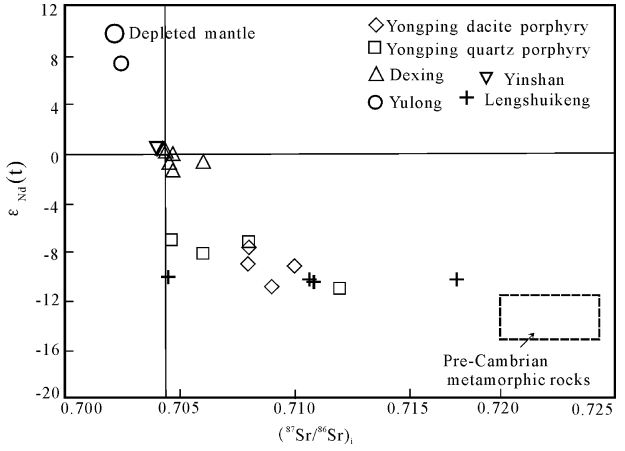


**Fig. 12** εNd(t)-ISr(t) diagram for both dacite and quartz porphyries. Data source: Dexing Cu–Mo deposit (JGEB, 1996); Yinshan Cu–Au–Pb–Zn–Ag deposit (JGEB, 1996); Lengshuikeng Pb–Zn–Ag deposit (Meng *et al*., 2007); Yulong Cu–Mo deposit (Jiang *et al*., 2006). Depleted mantle value and pre-cambrian metamorphic rocks are according to Zhu *et al*. (1990) and Shen *et al*. (1998).

data from the dacite porphyry and the quartz porphyry plot in the IV quadrant, again showing a mingling of magma sources between the mantle and the crust. In the diagram of $\varepsilon_{Nd}(t)$-t (Ma) (Fig. 13), all the data plot within the Meso-Proterozoic crustal evolution area, suggesting both the dacite porphyry and the quartz porphyry derived from partial melting of the Meso-Proterozoic crust. Two-stage model ages ($T_{DM2}$) of

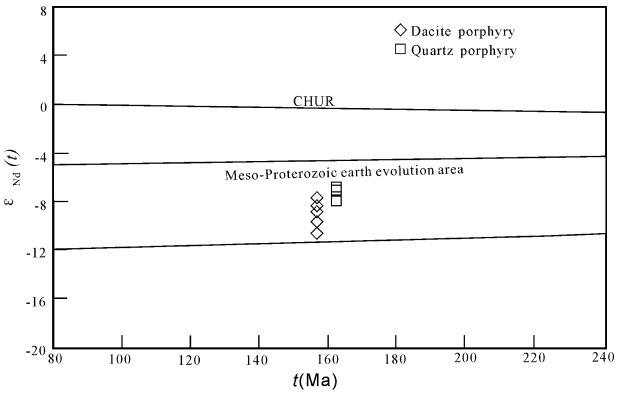


**Fig. 13** εNd(t)-t(Ma) diagram for both dacite and quartz porphyries (modified after Shen *et al*., 1998).

dacitie porphyry (1.58Ga–1.69Ga) and quartz porphyry (1.51Ga–1.84Ga) also indicate the contribution of Meso-Proterozoic crust to the magma sources. Compared with other ore-related porphyries, for example, the Dexing granodiorite porphyry and the Yinshan dacite porphyry in northeast Jiangxi Province, the ore-related porphyries at Yongping show characteristics of lower $\varepsilon_{Nd}$ (t) and older Nd model age (Wang *et al*., 2006). This may suggest that the source magmas were mixed in different proportions for quartz porphyry and dacite porphyry at the Yongping Cu–Mo–W deposit, Dexing porphyry Cu–Mo–Au, Yinshan polymetallic deposit, and Lengshuikeng Pb–Zn deposit (Fig. 12).

## 6.4 Implications for regional mineralization

The dacite and quartz porphyries at Yongping deposit are subduction-related high-K calc-alkaline series (Li *et al*., 2007a). The intrusive rocks at the Dexing porphyry Cu–Mo deposit, located in the northeast Jiangxi Province, about 100 km from the Yongping deposit (Fig. 1), also shows subduction-related magmatic arc characteristics, but the intrusive rocks at both deposits show different geochemical compositions. The intrusive rocks at both deposits are poor in Nb, Ta, and Ti contents, however, the intrusive rocks at the Dexing deposit are rich in Rb, Ba, Zr, Hf, Sr, and P, whereas intrusive rocks at the Yongping deposit is poor in Sr and P. This may reflect differences in their magma sources and in fractional crystallization. The ore-related porphyry in the Dexing Cu–Mo deposit shows adakite affinity, whereas the dacite and quartz porphyries in the Yongping deposit do not (Li & Watanabe, 2006). This suggests a difference in tectonic setting and source

materials of magma between ore-related intrusive rocks at the Dexing and Yongping deposits. Rb/Sr ratios of the intrusive rocks at the Dexing deposit (0.05–0.28) are lower than that of the porphyries in the Yongping deposit (Rb/Sr ratios of 0.35–1.12 for its dacite porphyry and Rb/Sr ratios of 1.59–9.29 for its quartz porphyry).

The zircon SHRIMP U–Pb age analysis of the dacite and quartz porphyries shows that the ore-related porphyries were emplaced at 160 Ma at the Yongping deposit. The molybdenite Re–Os ages show the Mo mineralization at 157 Ma at Yongping. Both the ore-related porphyries and the Cu–Mo mineralization occurred in the Late Jurassic time. The ages of the Dexing porphyry Cu–Mo deposit (zircon SHRIMP U-Pb age of 171 Ma and molybdenite Re–Os age of 170 Ma, Lu *et al*., 2005; Wang *et al*., 2006; Li *et al*., 2013) and the Yinshan polymetal deposit (zircon SHRIMP U–Pb age of 181 Ma and muscovite Ar–Ar age of 179 Ma) (Li *et al*., 2007b) are older than that of the Yongping deposit, although they are coeval with the large-scale W-Sn mineralization (for example, Shizhuyuan W–Sn deposit of 154.7 ± 2.5 Ma and Dangping W deposit of 154.9 ± 2.4 Ma) in southeast China. The Dexing porphyry Cu–Mo–Au and Yinshan polymetallic deposits are considered to be the products of an arc magmatism within a transpressional tectonic setting (Watanabe & Li, 2006; Li & Sasaki, 2007). The ore-related rocks with large-scale W–Sn mineralization in southeast China are mainly biotite granite (Hua *et al*., 2005). Obviously the differences in magma sources and in tectonic settings were accountable for production of different ore-related igneous rocks and deposits. It is suggested that the Yongping Cu–Mo deposit was produced during the transitional setting from a compressional tectonic regime to an extensional tectonic environment, while the southeast China underwent a widespread crustal extension in Late Jurassic Period (Hua *et al*., 2005).

## 7. Conclusions

This study reveals that the dacite and quartz porphyries at the Yongping deposit show similar REE patterns with subduction-related features, i.e., LILE-enrichment (Ba, Rb, and K) and HFSE (Th, Nb, Ta, and Ti) depletion. The zircon SHRIMP U-Pb ages indicate that the ore-related porphyries were emplaced at Late Jurassic. The inherited ages (432 Ma and 208.6 Ma) were generated by two metamorphic events. The inherited age of 766 Ma from an igneous zircon suggested a Neo-Proterozoic magmatic event in the Yongping district. The dating results of hydrothermal muscovite and biotite from the porphyries indicate that the Mo mineralization and the associated hydrothermal activity are coeval with the magmatic intrusions at Yongping. The Sr–Nd isotopic values for the dacite and quartz porphyries indicate a mixture magma source. The $\varepsilon_{Nd}(t)$ data from the dacite and quartz porphyries suggest a partial melting of the Meso-Proterozoic crust to contribute to the magma process. Comparing with the neighboring Dexing porphyry Cu–Mo and the Yinshan polymetallic deposits, as well as the Shizhuyuan and Dangping W deposits of south China in terms of their geochemical features and tectonic settings, it is proposed that the Yongping deposit was produced during the tectonic transition from a compressional tectonic regime to an extensional tectonic environment at the Late Jurassic.

## Acknowledgments

This study was financially supported by the National Fundamental Research Development Program of China (grant no. 2012CB416705), the National Natural Science Foundation of China (grant no. 41272112, 40872065), and the One Hundred Person Project of the Chinese Academy of Sciences. We thank Huang Zhenjin, Wei Xinglin for their assistance during our field seasons, and Professor Hideo Hirano for his kind help for samples thin sections descriptions. We are indebted to Zhangyan, Dong Huiyan, and Chen Zhenyu for their help with SHRIMP U–Pb analysis and CL imaging.

## References

Bacon, C. R. and Lowenstern, J. B. (2005) Late Pleistocene granodiorite source for recycled zircon and phenocrysts in rhyodacite lava at Crater Lake Oregon. Earth Planet. Sci. Lett., 233, 277–293.

Barra, F., Ruiz, J., Mathur, R. and Titley, S. (2003) A Re-Os study on sulfide minerals from the Bagdad porphyry Cu–Mo deposit, northern Arizona, USA. Mineral. Deposita, 38, 585–596.

Birck, J. L., RoyBarman, M. and Campas, F. (1997) Re-Os measurements at the femtomole level in natural samples. Geostandard Newslett., 20, 19–27.

Blichert-Toft, B. and Albarede, F. (1997) The Lu-Hf isotope geochemistry of chondrites and the evolution of the mantle-crust system. Earth Planet. Sci. Lett., 148, 243–258.

Chen, A. (1999) Mirror-image thrusting in the South China orogenic belt: tectonic evidence from western Fujian southeastern China. Tectonophysics, 305, 497–519.

Chen, W., Zhang, Y., Ji, Q., Wang, S. S. and Zhang, J. X. (2002) The magmatism and deformation times of the Xidatan rock series, East Kunlun Mountain. Sci. China (Ser. B), 45, 20–27.

Corfu, F. and Noble, S. R. (1992) Genesis of the southern Abitibi greenstone belt, Superior Province, Canada: evidence from zircon Hf isotope analyses using a single filament technique. Geochim. Cosmochim. Acta, 56, 2081–2097.

Ding, X., Jiang, S. Y., Ni, P., Gu, L. Y. and Jiang, Y. Y. (2005) Zircon SIMS U-Pb geochronology of host granitoids in Wushan and Yongping Copper Deposits, Jiangxi Province. Geol. J. China Univ., 11, 383–389 (in Chinese with English abstract).

Du, L. T. (2005) Sources of ore-forming material and genesis analysis of Yongping copper deposit. Jiangxi Resour. Environ. Eng., 19, 4–11 (in Chinese with English abstract).

Elburg, M. A. (1996) U-Pb ages and morphologies of zircon in microgranitoid enclaves and peraluminous host granite: evidence for magma mingling. Contrib. Mineral. Petrol., 123, 177–189.

Goldstein, S. L., O'Nions, R. K. and Hamilton, P. J. (1984) A Sm-Nd study of atmospheric dusts and particulates from major river systems. Earth Planet. Sci. Lett., 70, 221–236.

Griffin, W. L., Pearson, N. J., Belousova, E., Jackson, S. E., van Achterbergh, E., O'Reilly, S. Y. and Shee, S. R. (2000) The Hf isotope composition of cratonic mantle: LA-MC-ICPMS analysis of zircon megacrysts in kimberlites. Geochim. Cosmochim. Acta, 64, 133–147.

Gu, L. X. and Xu, K. Q. (1986) On the South China-type massive sulphide deposits formed on marine fault depression troughs on the continental crust. Miner. Deposits, 5, 1–13 (in Chinese with English abstract).

Hawkesworth, C. J., Turner, S. P., McDermott, F., Peate, D. W. and van Calsteren, P. (1997) U-Th isotopes in arc magmas: implications for element transfer from the subducted crust. Science, 276, 551–555.

He, J. (1993) Metallogenic geochemistry and genesis study on Yongping copper ore deposit of Jiangxi Province. Miner. Resour. Geol., 7, 1–7 (in Chinese with English abstract).

Hoskin, P. W. O. (1998) Minor and trace element analysis of natural zircon ($ZrSiO_4$) by SIMS and laser ablation ICP-MS: a consideration and comparison of two broadly competitive techniques. J. Trace Microprobe Tech., 16, 301–326.

Hoskin, P. W. O. and Schaltegger, U. (2003) The composition of zircon and igneous and metamorphic petrogenesis. Rev. Mineral. Geochem., 53, 2–62.

Hua, R. M., Chen, P. R., Zhang, W. L., Yao, J. M., Lin, J. F., Zhang, Z. S., Gu, S. Y., Liu, X. D. and Qi, H. W. (2005) Metallogenesis related to Mesozoic granitoids in the Nanling Range, south China and their geodynamic setting. Acta Geol. Sin., 79, 810–820.

Huang, C. K., Bai, Z., Zhu, Y. S., Wang, H. Z. and Shang, X. Z. (2001) Copper deposits in China. Geological Publishing House, Beijing, 705p (in Chinese with English abstract).

Iizuka, T. and Hirata, T. (2005) Improvements of precision and accuracy in in situ Hf isotope microanalysis of zircon using the laser ablation-MC-ICPMS technique. Chem. Geol., 220, 121–137.

Jahn, B. M. and Condie, K. C. (1995) Evolution of the Kaapvaal Craton as viewed from geochemical and Sm-Nd isotopic analyses of intracratonic pelites. Geochim. Cosmochim. Acta, 59, 2239–2258.

Jian, P., Liu, D. Y. and Sun, X. M. (2003) SHRIMP dating of Carboniferous Jinshajiang ophiolite in western Yunnan and Sichuan: geochronological constraints on the evolution of the paleo-Tethys oceanic crust. Acta Geol. Sin., 77, 217–277 (in Chinese with English abstract).

Jiang, Y. H., Jiang, S. Y., Lin, H. F. and Dai, B. Z. (2006) Low-degree melting of a metasomatized lithospheric mantle for the origin of Cenozoic Yulong monzogranite-porphyry, east Tibet: geochemical and Sr-Nd-Pb-Hf isotopic constraints. Earth Planet. Sci. Lett., 241, 217–233.

Jiangxi Geological Exploration Bureau (JGEB) (1996) Yinshan Cu-Pb-Zn-Ag deposit in Jiangxi Province. Geological Publising House, Beijing, 380p (in Chinese with English abstract).

Kirwin D. 2005. Unidirectional solidification textures associated with intrusion-related Mongolian mineral deposits. *In* Seltmann, R., Gerel, O. and Kirwin, D. J. (eds). Geodynamics and metallogeny of Mongolia with a special emphasis on copper and gold deposits. National Historical Museum, London, 63–84.

Kirwin D. 2006. Unidirectional solidification textures, miarolitic cavities and orbicles: field evidence for the magmatic to hydrothermal transition in intrusion-related mineral deposit Proceedings of 19th General Meeting of the International Mineralogical Association, 185.

Li, X. F. and Sasaki, M. (2007) The hydrothermal alteration and mineralization of Middle Jurassic Dexing porphyry Cu–Mo deposit, Southeast China. Resour. Geol., 57, 409–426.

Li, X. F. and Watanabe, Y. (2006) Hydrothermal alteration and mineralization of Dexing porphyry copper deposit, South China. Proceeding of 19th General Meeting of the International Mineralogical Association, 186.

Li, X. F., Hu, R., Rusk, B., Xiao, R., Wang, C. Z., Yang, F. (2013) U-pb and Ar-Ar geochronology of the Fujiawu porphyry Cu-Mo deposit, Dexing district, Southeast China: Implications for magmatism, hydrothermal alteration, and mineralization. J. Asian Earth Sci., doi:http://dx.doi.org/10.1016/j.jseaes.2013.04.012

Li, X. F., Watanabe, Y. and Qu, W. J. (2007a) Texture and geochemical characteristics of granitic rocks in the Yongping climax-type Cu–Mo deposit, Jiangxi, Southeastern China, and their alteration and mineralization. Acta Petrol. Sin., 23, 2353–2365 (in Chinese with English abstract).

Li, X. F., Watanabe, Y., Mao, J. W., Chen, Z. Y., Liu, S. X. and Yi, X. K. (2007b) SHRIMP U-Pb zircon and $^{40}Ar$-$^{39}Ar$ muscovite ages in the Yinshan deposit in the Northeast Jiangxi Province, South China. Resour. Geol., 57, 325–337.

Liao, Z. T. and Liu, J. S. (2003) Evidence of submarine volcanic hydrothermal sediment mineralization in Yongping copper deposit. Eng. Copper, 1, 31–35 (in Chinese with English abstract).

Liu, X. and Huang, Z. (1991) The discussion on the development of structures at Yongping Cu deposit in Jiangxi province. Miner. Resour. Geol., 5, 416–422 (in Chinese).

Lu, J. J., Hua, R. M. and Yao, C. L. (2005) Re-Os age for molybdenite from the Dexing porphyry Cu-Au deposit of Jiangxi Province, China. Geochim. Cosmochim. Acta (Suppl.), 69, A882.

Ludwig, K. R. (2001) User's manual for isoplot/Ex.Version 2.47. A geochronological tool for Microsoft Excel. Berkeley Geochronology Center, Berkeley, 43p.

Lugmair, G. W. and Marti, K. (1978) Lunar initial $^{143}Nd/^{144}Nd$: differential evolution of the lunar crust and mantle. Earth Planet. Sci. Lett., 39, 349–357.

Mathur, R., Marschik, R., Ruiz, J., Munizaga, F. and Leveille, R. (2002) Age of mineralization of the Candelaria iron oxide Cu-Au deposit, and the origin of the Chilean Iron Belt based on Re-Os isotopes. Econ. Geol., 97, 59–71.

Meng, X. J., Dong, G. Y. and Liu, J. G. (2007) Lengshuikeng porphyry Pb-Zn-Ag deposit in Jiangxi Province. Geological Publishing House, Beijing, 135p.

Nagler, T. F. and Frei, R. (1997) Plug in plug osmium distillation. Schweiz Miner. Petrogr. Mitt., 77, 123–127.

Nowell, G. M., Kempton, P. D., Noble, S. R., Fitton, J. F., Saunders, A. D., Mahoney, J. J. and Taylor, R. N. (1998) High precision Hf isotope measurements of MORB and OIB by thermal ionisation mass spectrometry: insights into the depleted mantle. Chem. Geol., 149, 211–233.

Peucat, J. J., Vidal, P., Bernard-Griffiths, J. and Condie, K. C. (1989) Sr, Nd and Pb isotopic systematics in the Archaean low- to high grade transition zone of southern India: syn-accretion vs. post-accretion granulites. J. Geol., 97, 537–550.

Ren, J. G. (1994) The genesis and structure control of Yongping copper deposit, Jiangxi. Eng. Copper, 3, 35–40 (in Chinese with English abstract).

Rubatto, D. (2002) Zircon trace element geochemistry: partitioning with garnet and the link between U-Pb ages and metamorphism. Chem. Geol., 184, 123–138.

Shen, W. Z., Lin, H. F., Li, W. X., Wang, D. Z., Huang, X. and Pan, J. (1998) The Sm-Nd isotopic composition of Mesozic granite in Jiangxi province. Chin. Sci. Bull., 43 (24), 2653–2657.

Smoliar, M., Walker, R. and Morgan, J. (1996) Re-Os of group IIA, IIIA, VA, IVB iron meteorites. Science, 271, 1099–1102.

Steiger, R. H. and Jäger, E. (1977) Subcommission on geochronology: convention on the use of decay constants in geo- and cosmochronology. Earth Planet. Sci. Lett., 36, 359–362.

Stevenson, R. K. and Patchett, P. J. (1990) Implications for the evolution of continental crust from Hf isotope systematics of Archean detrital zircons. Geochim. Cosmochim. Acta, 54, 1683–1697.

Sun, S. S. and McDonough, W. F. (1989) Chemical and isotopic systematics of oceanic basalts: implications for mantle composition and processes. *In* Saunders, A. D. and Norry, M. J. (eds.) Magmatism in the ocean basins., Vol. 42. Geological Society Special Publications, London, 313–345.

Wang, Q., Xu, J. F., Jian, P., Bao, Z. W., Zhao, Z. H., Li, C. F., Xiong, X. L. and Ma, J. L. (2006) Petrogenesis of adakiic porphyries in an extensional tectonic setting, Dexing, South China: implications for the genesis of porphyry copper mineralization. J. Petrol., 47, 119–144.

Watanabe, Y. and Li, X. F. (2006) Tectonic setting of Dexing porphyry Cu–Mo deposit in south China: transitional setting from magmatic arc to contraction zone. Proceeding of 19th General Meeting of the International Mineralogical Association, 186.

Wu, F. Y., Yang, Y. H. and Xie, L. W. (2006) Hf isotopic compositions of the standard zircons and baddeleyites used in U-Pb geochronology. Chem. Geol., 234, 105–126.

Xu, P., Fan, Q. C. and O'Reilly, S. Y. (2004) Hf isotopic compositions of the standard zircons for U-Pb dating. Chin. Phys. Lett., 49, 1642–1648.

Zhang, Z. Q., Liu, D. Y. and Fu, G. M. (1994) Studying on Isotopic Geochronology of Metamorphic Rocks in the Northern Qinling. Geological Publishing House, Beijing, 232p (in Chinese with English abstract).

Zhu, J. C., Shen, W. Z., Liu, C. S. and Xu, S. J. (1990) Nd-Sr isotopic characteristics and genetic discussion of Mesozoic granitiods of syntexis series in South China. Acta Petrol. Mineral., 9, 97–105.